Title: Preproglucagon (PPG) neurons innervate neurochemically identified autonomic neurons in the mouse brainstem

Corresponding Author: Dr Stefan Trapp,

Corresponding Author's Institution: Imperial College

First Author: Ida J Llewellyn-Smith, PhD

Order of Authors: Ida J Llewellyn-Smith, PhD; Greta J Gnanamanickam; Frank Reimann; Fiona M Gribble; Stefan Trapp, PhD

Abstract: Preproglucagon (PPG) neurons produce glucagon-like peptide-1 (GLP-1) and occur primarily in the nucleus tractus solitarius (NTS). GLP-1 affects a variety of central autonomic circuits, including those controlling the cardiovascular system, thermogenesis, and most notably energy balance. Our immunohistochemical studies in transgenic mice expressing YFP under the control of the PPG promoter showed that PPG neurons project widely to central autonomic regions, including brainstem nuclei. Functional studies have highlighted the importance of hindbrain receptors for the anorexic effects of GLP-1.

In this study, we assessed YFP innervation of neurochemically-identified brainstem neurons in transgenic YFP-PPG mice. Immunoreactivity for YFP plus choline acetyltransferase (ChAT), tyrosine hydroxylase (TH) and/or serotonin (5-HT) were visualised with two- or three-colour immunoperoxidase labelling using black (YFP), brown and blue-grey reaction products.

In the dorsal motor nucleus of the vagus (DMV), terminals from fine YFP-immunoreactive axons closely apposed a small proportion of ChAT-positive and rare TH-positive/ChAT-positive motor neurons, mostly ventral to AP. YFP-immunoreactive innervation was virtually absent from the compact and loose formations of the nucleus ambiguus. In the NTS, some TH-immunoreactive neurons were closely apposed by YFP-containing axons. In the A1/C1 column in the ventrolateral medulla, close appositions on TH-positive neurons were more common, particularly in the caudal portion of the column. A single YFP-immunoreactive axon usually provided 1-3 close appositions on individual ChAT- or TH-positive neurons. Serotonin-immunoreactive neurons were most heavily innervated, with the majority of raphé pallidus, raphé obscurus and parapyramidal neurons receiving several close appositions from large varicosities of YFP-immunoreactive axons.

These results indicate that GLP-1 neurons innervate various populations of brainstem autonomic neurons. These include vagal efferent neurons and catecholamine neurons in areas linked with cardiovascular control. Our data also indicate a synaptic connection between GLP-1 neurons and 5-HT neurons, some of which might contribute to the regulation of appetite.

Response to Reviewers: We thank the Reviewers for their thorough evaluation of our manuscript and their helpful suggestions, which have improved the manuscript significantly. We now provide a revised manuscript that incorporates the suggestions of the Reviewers and hope that it is now acceptable for publication in Neuroscience.

Below are our detailed responses to each point raised by the Reviewers:

REVIEWER #1,

1) "The presentation of the data is inadequate. The data are important and the authors stress several times that the powerful immunohistochemistry of YFP has enabled them to view the complete brainstem PPG innervation. If this is indeed the case - and I must admit that the staining shown in Figs 1-3 is really clear - they should help the reader in understanding the full extent of this innervation. This could be done in a series of line-drawings through the caudal brainstem (e.g. using images from mouse brain atlases) illustrating the location of 5HT, ChAT and TH cells (could even be illustrated on the same images) and the degree of innervation by PPG/YFP fibers. It is very difficult from the rather selected illustrations to get a full picture of the brainstem innervation and the extent to which the different phenotypically labeled neurons are contacted by the YFP fibers."

- We have added three new figures to the revised manuscript (Figures 2, 4 and 6). The new figures show maps of the distributions of TH-immunoreactive, ChAT-immunoreactive and 5-HT-immunoreactive neurons in sections through various regions of the medulla. The maps indicate which neurons receive close appositions from YFP-immunoreactive varicosities and which do not and include counts of the neurons with and without appositions. The inclusion of three new figures in the revised manuscript has required us to add a section to Experimental Procedures describing how the maps were constructed and neurons were counted (section 2.2.1, "Mapping neurochemically-identified brainstem neurons that received or lacked YFP-immunoreactive innervation" on pages 10 and 11).
    These new figures and the quantitative data have substantially strengthened the manuscript. We thank Reviewer #1 for suggesting that we include such figures.

2) "The data are heavily overinterpreted: The two last highlights are overstatements that are not supported by the data":
    "The first statement is not supported by the data - and it certainly does not explain the cardiovascular effects of GLP-1 - well it could potentially be a route by which GLP-1 influences the cardiovascular system, but the authors do not know if this is an important pathway."
    "The second statement is also heavily overinterpretation. Yes - GLP-1 is involved in appetite regulation and so is the serotonergic system, but if the two are connected and if the serotonergic neurons contacted by YFP fibers are involved in satiation (or one of the other multiple functions of serotonin) remains to be determined. I think the authors based on the data presented needs to be a little more careful when interpreting the interconnection between GLP-1 and serotonin. This should also be reflected in the discussion."

- We agree with Reviewer #1 and have now reformulated to make clearer that our statements in the highlights are speculative. We would, however, like to keep these interpretative statements, as they might attract a wider audience.

"Overall, while it is impossible that GLP-1 and 5HT are interconnected there is no evidence in the current paper that this is the case." "Because GLP-1 and 5HT are both involved in appetite regulation does not automatically imply that the one systems works via the other."

We have altered the Discussion accordingly (section 4.4, pages 19 and 20).

OTHER ISSUES:

1) "On Page 10 the authors give a long description of how they tested for the specificity of the 5-HT antibody: "We tested the specificity of the anti-5-HT antiserum by adsorbing it with a glutaraldehyde conjugate of 5-HT and keyhole limpet haemocyanin (KLH). To prepare the 5-HT-glutaraldehyde-KLH conjugate, 50 mg of KLH (Catalogue #H-2133, Lot #43H9524;"
     "This entire section can be removed. 5HT staining is widely used and the use of a commercially antibody giving the correct pattern of staining is in my view sufficient documentation for specificity."

- We have done as Reviewer #1 suggested and removed this section.

2) "Table 3 should be omitted and the antibodies and lot numbers could be included in the main text."

- As suggested, we have removed Table 3 and included the information in the text of the revised manuscript.

REVIEWER #2:

"While the goals of the work are important and the YFP-PPG mouse valuable for a variety of experimental endpoints, enthusiasm for the MS is significantly diminished by the absence of quantification in light microscopic analysis, the small numbers of projections to neurons in target regions other than the caudal raphe, and the lack of additional knowledge about neurons that receive close appositions from YFP-PPG neurons (e.g., as noted by authors on P 16 line 16-17 regarding the tracing experiments required to reveal whether particular DMV neurons are enroute to affect to stomach versus pancreas)."

- We have added three new figures containing maps of neurons with and without close appositions from YFP-immunoreactive axons and quantification (see response to Reviewer #1).

ADDITIONAL COMMENTS.

"The authors note on P 14 line 38-39 that only EM can provide proof of functional contacts. They then mention a finding from Pilowsky et al. that provides a perspective for their statement that half of the light microscopically determined terminals are revealed to make synaptic contacts based on EM analysis. Given this rule of thumb, the general sparseness (all based on qualitative terms such as few, sparse, a very small number, etc) of YFP projections to ChAT and to TH neurons only served to further qualify conclusions that might be drawn from the present results. In addition, given the concern about using instances of close apposition based on light microscopic data I am puzzled by the absence of quantifying their findings for each brainstem nucleus examined."

- We have now added quantification in Figures 2, 4, and 6 - see response to Reviewer #1.

"The 5-HT positive neurons of the caudal raphe receive qualitatively more YFP projections than other targets. When talking about the possible functional meaning of such projections the authors conclude

(in Abst.) that this connection may contribute to the regulation of appetite. No further support or elaboration of it is made in the Discussion. In addition, given the extensive literature on raphe pallidus contribution to brown fat thermogenesis, the hypothermic effect of central GLP-1R agonist, and YFP input to raphe pallidus revealed here, it was puzzling that no functional comments were made."

- We have expanded on the possible link to thermogenesis, as suggested by Reviewer #2. Please see section 4.4 of the Discussion in the revised manuscript (pages 19 and 20) .

"The abstract and introduction state that PPG neurons produce the satiety peptide GLP-1. Given the range of effects of GLP-1 including GI motility, incretin, cardiovascular and other effects to describe the peptide with this functional label is misleading."

- We have changed the abstract accordingly.

Dear Prof Lisberger,

RE: NSC 12-587

We submit for your consideration for publication in *Neuroscience* a revised version of our article entitled '**Preproglucagon (PPG) neurons innervate neurochemically identified autonomic neurons in the mouse brainstem'** by *Llewellyn-Smith, Gnanamanickam, Reimann, Gribble & Trapp*.

The manuscript has been modified on the basis of the suggestions of the Reviewers. In particular, we have included 3 new figures in addition to the three figures in the original version of the manuscript. The new figures document the distributions in the medulla of cholinergic, catecholaminergic and serotonergic neurons that receive or lack close appositions from YFP-PPG axons.

We have uploaded colour versions of all 6 Figures. If the revised manuscript is accepted for publication in Neuroscience, we would like all of the Figures to be published in colour online. However, in print, Figures 2-5 should appear in black and white as colour reproduction is only essential for Figure 1. In the revised manuscript, we have included two versions of the Figure Legends. The Legends that should appear in the online version of the article ("Figure Legends (ONLINE VERSION)", pages 21-24) describe the six figures in colour. The Legends that should appear in the print version of the article ("Figure Legends (PRINT VERSION)", pages 24-26) describe the colour version of Figure 1 and the black and white versions of Figures 2-5.

Thank you very much for your consideration. We look forward to hearing from you about the manuscript in due course.

Yours sincerely,

Dr Stefan Trapp
Department of Surgery and Cancer
Imperial College London
On behalf of the authors

<u>***Manuscript NSC-12-587*** *- Response to Reviewers*</u>

We thank the Reviewers for their thorough evaluation of our manuscript and their helpful suggestions, which have improved the manuscript significantly. We now provide a revised manuscript that incorporates the suggestions of the Reviewers and hope that it is now acceptable for publication in Neuroscience.

Below are our detailed responses to each point raised by the Reviewers:

REVIEWER #1,

1*) "The presentation of the data is inadequate. The data are important and the authors stress several times that the powerful immunohistochemistry of YFP has enabled them to view the complete brainstem PPG innervation. If this is indeed the case - and I must admit that the staining shown in Figs 1-3 is really clear - they should help the reader in understanding the full extent of this innervation. This could be done in a series of line-drawings through the caudal brainstem (e.g. using images from mouse brain atlases) illustrating the location of 5HT, ChAT and TH cells (could even be illustrated on the same images) and the degree of innervation by PPG/YFP fibers. It is very difficult from the rather selected illustrations to get a full picture of the brainstem innervation and the extent to which the different phenotypically labeled neurons are contacted by the YFP fibers."*

- We have added three new figures to the revised manuscript (Figures 2, 4 and 6). The new figures show maps of the distributions of TH-immunoreactive, ChAT-immunoreactive and 5-HT-immunoreactive neurons in sections through various regions of the medulla. The maps indicate which neurons receive close appositions from YFP-immunoreactive varicosities and which do not and include counts of the neurons with and without appositions. The inclusion of three new figures in the revised manuscript has required us to add a section to Experimental Procedures describing how the maps were constructed and neurons were counted (section 2.2.1, "Mapping neurochemically-identified brainstem neurons that received or lacked YFP-immunoreactive innervation" on pages 10 and 11).
     These new figures and the quantitative data have substantially strengthened the manuscript. We thank Reviewer #1 for suggesting that we include such figures.

2*) "The data are heavily overinterpreted: The two last highlights are overstatements that are not supported by the data":*
     "The first statement is not supported by the data - and it certainly does not explain the cardiovascular effects of GLP-1 - well it could potentially be a route by which GLP-1 influences the cardiovascular system, but the authors do not know if this is an important pathway."
     "The second statement is also heavily overinterpretation. Yes - GLP-1 is involved in appetite regulation and so is the serotonergic system, but if the two are connected and if the serotonergic neurons contacted by YFP fibers are involved in satiation (or one of the other multiple functions of serotonin) remains to be determined. I think the authors based on the data presented needs to be a little more careful when interpreting the interconnection between GLP-1 and serotonin. This should also be reflected in the discussion."

-   We agree with Reviewer #1 and have now reformulated to make clearer that our statements in the highlights are speculative. We would, however, like to keep these interpretative statements, as they might attract a wider audience.

"Overall, while it is impossible that GLP-1 and 5HT are interconnected there is no evidence in the current paper that this is the case."   "Because GLP-1 and 5HT are both involved in appetite regulation does not automatically imply that the one systems works via the other."

We have altered the Discussion accordingly (section 4.4, pages 19 and 20).

OTHER ISSUES:

1) *"On Page 10 the authors give a long description of how they tested for the specificity of the 5-HT antibody: "We tested the specificity of the anti-5-HT antiserum by adsorbing it with a glutaraldehyde conjugate of 5-HT and keyhole limpet haemocyanin (KLH). To prepare the 5-HT-glutaraldehyde-KLH conjugate, 50 mg of KLH (Catalogue #H-2133, Lot #43H9524;"*
    "This entire section can be removed. 5HT staining is widely used and the use of a commercially antibody giving the correct pattern of staining is in my view sufficient documentation for specificity."

- We have done as Reviewer #1 suggested and removed this section.

2*) "Table 3 should be omitted and the antibodies and lot numbers could be included in the main text."*

- As suggested, we have removed Table 3 and included the information in the text of the revised manuscript.

REVIEWER #2:

"While the goals of the work are important and the YFP-PPG mouse valuable for a variety of experimental endpoints, enthusiasm for the MS is significantly diminished by the absence of quantification in light microscopic analysis, the small numbers of projections to neurons in target regions other than the caudal raphe, and the lack of additional knowledge about neurons that receive close appositions from YFP-PPG neurons (e.g., as noted by authors on P 16 line 16-17 regarding the tracing experiments required to reveal whether particular DMV neurons are enroute to affect to stomach versus pancreas)."

- We have added three new figures containing maps of neurons with and without close appositions from YFP-immunoreactive axons and quantification (see response to Reviewer #1).

ADDITIONAL COMMENTS.

"The authors note on P 14 line 38-39 that only EM can provide proof of functional contacts. They then mention a finding from Pilowsky et al. that provides a perspective for their statement that half of the light microscopically determined terminals are revealed to make synaptic contacts based on EM analysis. Given this rule of thumb, the general sparseness (all based on qualitative terms such as few, sparse, a very small number, etc) of YFP projections to ChAT and to TH neurons only served to further qualify conclusions that might be drawn from the present results. In addition, given the concern about using instances of close apposition based on light microscopic data I am puzzled by the absence of quantifying their findings for each brainstem nucleus examined."

- We have now added quantification in Figures 2, 4, and 6 - see response to Reviewer #1.

"The 5-HT positive neurons of the caudal raphe receive qualitatively more YFP projections than other targets. When talking about the possible functional meaning of such projections the authors conclude (in Abst.) that this connection may contribute to the regulation of appetite. No further support or elaboration of it is made in the Discussion. In addition, given the extensive literature on raphe pallidus contribution to brown fat thermogenesis, the

hypothermic effect of central GLP-1R agonist, and YFP input to raphe pallidus revealed here, it was puzzling that no functional comments were made.”

- We have expanded on the possible link to thermogenesis, as suggested by Reviewer #2. Please see section 4.4 of the Discussion in the revised manuscript (pages 19 and 20) .

“The abstract and introduction state that PPG neurons produce the satiety peptide GLP-1. Given the range of effects of GLP-1 including GI motility, incretin, cardiovascular and other effects to describe the peptide with this functional label is misleading.”

- We have changed the abstract accordingly.

HIGHLIGHTS

- GLP-1 neurons directly innervate brainstem cholinergic and monoaminergic neurons.

- GLP-1 may influence satiety via heavy GLP-1 innervation of brainstem 5-HT neurons.

- Innervation of dorsal vagal neurons underpins GLP-1's role in control of digestion.

- Central GLP-1 may affect cardiovascular control via GLP-1 inputs to C1 neurons.

1
2
3
4
5
6
7
8
9
10
11
12
13
14
15
16
17
18
19
20
21
22
23
24
25
26
27
28
29
30
31
32
33
34
35
36
37
38
39
40
41
42
43
44
45
46
47
48
49
50
51
52
53
54
55
56
57
58
59
60
61
62
63
64
65

PREPROGLUCAGON (PPG) NEURONS INNERVATE NEUROCHEMICALLY IDENTIFIED AUTONOMIC NEURONS IN THE MOUSE BRAINSTEM

Ida J Llewellyn-Smith[1], Greta J. E. Gnanamanickam[1], Frank Reimann[2], Fiona M Gribble[2] & Stefan Trapp[3]

[1]Cardiovascular Medicine, Physiology and Centre for Neuroscience, Flinders University, Bedford Park SA 5042, Australia
[2]Cambridge Institute for Medical Research; Wellcome Trust/MRC Building, Addenbrooke's Hospital, Hills Road, Cambridge, CB2 2XY, UK
[3]Department of Surgery and Cancer & Cell Biology Section; South Kensington Campus, Imperial College, London, SW7 2AZ, UK

Abbreviated title: GLP-1 innervation of brainstem neurons

Section Editor: Dr Menno Witter

Corresponding author: Dr Stefan Trapp
SAF Building, Room 374a
Cell Biology Section
South Kensington Campus
Imperial College London
London
SW7 2AZ
Phone: ++44 (0)20 7594 7912
Email: s.trapp@imperial.ac.uk

ABSTRACT

Preproglucagon (PPG) neurons produce glucagon-like peptide-1 (GLP-1) and occur primarily in the nucleus tractus solitarius (NTS). GLP-1 affects a variety of central autonomic circuits, including those controlling the cardiovascular system, thermogenesis, and most notably energy balance. Our immunohistochemical studies in transgenic mice expressing YFP under the control of the PPG promoter showed that PPG neurons project widely to central autonomic regions, including brainstem nuclei. Functional studies have highlighted the importance of hindbrain receptors for the anorexic effects of GLP-1.

In this study, we assessed YFP innervation of neurochemically-identified brainstem neurons in transgenic YFP-PPG mice. Immunoreactivity for YFP plus choline acetyltransferase (ChAT), tyrosine hydroxylase (TH) and/or serotonin (5-HT) were visualised with two- or three-colour immunoperoxidase labelling using black (YFP), brown and blue-grey reaction products.

In the dorsal motor nucleus of the vagus (DMV), terminals from fine YFP-immunoreactive axons closely apposed a small proportion of ChAT-positive and rare TH-positive/ChAT-positive motor neurons, mostly ventral to AP. YFP-immunoreactive innervation was virtually absent from the compact and loose formations of the nucleus ambiguus. In the NTS, some TH-immunoreactive neurons were closely apposed by YFP-containing axons. In the A1/C1 column in the ventrolateral medulla, close appositions on TH-positive neurons were more common, particularly in the caudal portion of the column. A single YFP-immunoreactive axon usually provided 1-3 close appositions on individual ChAT- or TH-positive neurons. Serotonin-immunoreactive neurons were most heavily innervated, with the majority of raphé pallidus, raphé obscurus and parapyramidal neurons receiving several close appositions from large varicosities of YFP-immunoreactive axons.

These results indicate that GLP-1 neurons innervate various populations of brainstem autonomic neurons. These include vagal efferent neurons and catecholamine neurons in areas linked with cardiovascular control. Our data also indicate a synaptic connection between GLP-1 neurons and 5-HT neurons, some of which might contribute to the regulation of appetite.

KEY WORDS

glucagon-like peptide 1, nucleus of the solitary tract, tyrosine hydroxylase, choline acetyltransferase, serotonin, green fluorescent protein

HIGHLIGHTS

- GLP-1 neurons directly innervate brainstem cholinergic and monoaminergic neurons.

- GLP-1 may influence satiety via heavy GLP-1 innervation of brainstem 5-HT neurons.

- Innervation of dorsal vagal neurons underpins GLP-1's role in control of digestion.

- Central GLP-1 may affect cardiovascular control via GLP-1 inputs to C1 neurons.

LIST OF ABBREVIATIONS

5-HT	Serotonin, 5-hydroxytryptamine
AP	Area postrema
ChAT	Choline acetyltransferase
DAB	Diaminobenzidine
DMH	Dorsomedial nucleus of the hypothalamus
DMV	Dorsal motor nucleus of the vagus
GFP	Green fluorescent protein
GLP-1	Glucagon-like peptide 1
Ig	Immunoglobulin
IRT	Intermediate reticular nucleus
KLH	Keyhole limpet haemocyanin
LPS	Lipopolysaccharide
NA	Nucleus ambiguus
NHS	Normal horse serum
NTS	Nucleus of the solitary tract
PPG	Preproglucagon
PPY	Parapyramidal region
PVN	Paraventricular nucleus of the hypothalamus
RVLM	Rostral ventrolateral medulla
TH	Tyrosine hydroxylase
YFP	Yellow fluorescent protein

INTRODUCTION

Glucagon-like peptide 1 (GLP-1) is an incretin that is released from enteroendocrine cells and facilitates absorption of nutrients (Holst, 2007). Like other gut peptides, such as cholecystokinin, GLP-1 is also synthesized by neurons within the central nervous system. GLP-1 is produced by post-translational processing of preproglucagon (PPG) and immunoreactivity for the products of PPG processing is found in many brain regions, with highest levels occurring in the dorsomedial (DMH) and paraventricular nucleus (PVN) of the hypothalamus and lowest levels in the cortex and hindbrain (Jin et al., 1988, Vrang et al., 2007, Tauchi et al., 2008). Somata capable of synthesizing GLP-1, however, are restricted to the lower brainstem. The largest population of GLP-1-containing somata occurs in the caudal nucleus of the solitary tract (NTS) and there are also some cell bodies in the dorsomedial part of the medullary reticular nucleus (Jin et al., 1988, Larsen et al., 1997). Similarly, *in situ* hybridisation has revealed PPG mRNA only in the caudal NTS, the intermediate reticular nucleus (IRT) and the olfactory bulb (Merchenthaler et al., 1999). Retrograde tracing has confirmed that the hypothalamic axons containing GLP-1 arise from the cell bodies in the NTS and IRT (Larsen et al., 1997, Vrang et al., 2007).

Microinjection of GLP-1 or GLP-1 agonists into the brain has a multitude of effects, including suppression of food intake, control of blood glucose levels, nausea, changes in blood pressure and heart rate, as well as neuroprotection and effects on learning and memory (Tang-Christensen et al., 1996, Turton et al., 1996, Van Dijk et al., 1996, Thiele et al., 1998, Kinzig et al., 2002, Yamamoto et al., 2002, During et al., 2003, Cabou et al., 2008, Sandoval et al., 2008). Because of the functional importance of GLP-1 in the brain, we recently reinvestigated the distribution of central neurons capable of synthesizing GLP-1 using a transgenic mouse in which GLP-1 neurons express yellow fluorescent protein (YFP) throughout their cytoplasm under the control of the PPG promoter (Reimann et al., 2008). This approach allowed us to visualise PPG neurons and their processes with an unprecedented level of detail. Our study revealed the full distribution of PPG cell bodies and dendrites within the medulla and demonstrated that axons were widespread throughout the brain with the notable exception of cerebellum, hippocampus and cerebral cortex (Llewellyn-Smith et al., 2011). These observations matched well with the distribution of GLP-1 receptors within the brain (Shughrue et al., 1996, Merchenthaler et al., 1999). Notably, we found varicose axons in many central sites that are involved in regulating autonomic functions.

GLP-1 released in these areas could contribute to the global and coordinated control of food intake, energy balance and maintenance of cardiovascular homeostasis.

Recent functional studies have highlighted the importance of brainstem circuitry and brainstem GLP-1 receptors for physiological function (Yamamoto et al., 2003, Wan et al., 2007a, Wan et al., 2007b, Hayes et al., 2008, Hayes et al., 2009, Holmes et al., 2009, Williams et al., 2009, Barrera et al., 2011) see also (Trapp and Hisadome, 2011) for review). These findings, together with the fact that our immunohistochemical study revealed many more varicose immunoreactive axons in the brainstem than previously reported, prompted us to define the innervation targets of PPG neurons within the brainstem in more detail. Catecholamine neurons in the area postrema (AP) have been shown to express GLP-1 receptors (Yamamoto et al., 2003) and a subpopulation of cholinergic dorsal vagal motor neurons responds electrically to GLP-1 (Wan et al., 2007a, Wan et al., 2007b, Holmes et al., 2009), consistent with these cell types receiving inputs from GLP-1 neurons.

In this study, we used transgenic YFP-PPG mice (Reimann et al., 2008) in order to take advantage of the strong YFP expression that occurs throughout the cytoplasm of PPG neurons, including their terminals (Hisadome et al., 2010, Llewellyn-Smith et al., 2011). To reveal GLP-1 innervation of cholinergic, catecholamine and serotonin neurons in the brainstem, we detected YFP-immunoreactivity in combination with immunoreactivity for choline acetyltransferase (ChAT), tyrosine hydroxylase (TH) or 5-hydroxytryptamine (5-HT), using two-colour or three-colour immunoperoxidase staining.

2.   EXPERIMENTAL PROCEDURES

These studies were performed on 11 adult male and 11 adult female mGLU-124 Venus YFP mice (Reimann et al., 2008), which will be referred to here as YFP-PPG mice. Mice were perfused at 12-16 weeks of age and weighed between 25 and 35g with males consistently being heavier than females of the same age. Mice were bred at Imperial College, kept on a 12 hour light:dark cycle and had unlimited access to food and water. All experiments were carried out in accordance with the UK Animals (Scientific Procedures) Act, 1986, with appropriate ethical approval.

Mice under halothane anesthesia were given heparin (500 IU/l), flushed with phosphate-buffered saline to remove blood and perfused transcardially with 60 ml of phosphate-buffered 4% formaldehyde, pH 7.4. Brains were post-fixed intact for 3 days at

room temperature on a shaker in the same fixative and then shipped to Flinders for sectioning and immunohistochemical staining.

Blocks containing the brainstem were trimmed from the post-fixed brains and infiltrated with sucrose. Three series of transverse 30μm cryostat sections were cut from each block. Because we did not use a matrix to block the brains, the dorsoventral tilt of the sections varied among mice. Consequently, Bregma values could not be reliably assigned to the brainstem sections studied here.

2.1   IMMUNOHISTOCHEMISTRY

Cryostat sections were first washed 3 x 10 min in 10 mM Tris, 0.9% NaCl, 0.05% thimerosal in 10 mM phosphate buffer, pH 7.4, (TPBS) containing 0.3% Triton X-100 and then exposed to TPBS-Triton containing 10% normal horse serum (NHS) for at least 30 min. TPBS-Triton containing 10% NHS was used to dilute primary antibodies; TPBS-Triton containing 1% NHS, to dilute secondary antibodies; and TPBS-Triton, to dilute the avidin-horseradish peroxidase complex. All steps in each protocol occurred on a shaker at room temperature and 3 x 10 min washes in TPBS were done after each incubation in an immunoreagent.

Titration was used to determine the working concentrations of primary antibodies. Optimal dilutions produced the maximum number of immunoreactive structures with minimal non-specific background staining. In the case of the anti-green fluorescent protein (GFP) antibody used to detect the YFP-expressing neurons, more dilute antibody was used to optimally visualize axons than for optimally visualizing cell bodies (see Llewellyn-Smith et al., 2011). We have previously shown that mouse tissue lacking GFP-expressing neurons shows no staining after immunoperoxidase processing to reveal GFP (Llewellyn-Smith et al., 2011).

After completion of the double or triple-labelling immunoperoxidase protocol detailed below, sections were mounted in serial order onto chrome alum-gelatine coated slides, dried and dehydrated. Coverslips were applied with Permaslip mounting medium (Alban Scientific, St Louis MO, USA).

2.1.1.   Two-colour Immunoperoxidase Labelling

Double immunoperoxidase labelling was used to localise YFP-immunoreactivity with a black reaction product and either ChAT-, TH- or 5-HT-immunoreactivity with a brown

reaction product. After treatment with TBS-Triton and 10% NHS-TBS-Triton, the sections were transferred into 1:50,000 or 1:100,000 chicken anti-GFP (Catalogue #ab13970, Lot #623923; Abcam, Cambridge, UK) for 3-5 days. After washing, the sections were exposed overnight to 1:500 biotinylated donkey anti-chicken immunoglobulin (Ig) Y (Catalogue #703-065-155, ; Jackson ImmunoResearch, West Grove PA) and then to 1:1,500 ExtrAvidin-peroxidase (Sigma-Aldrich, St Louis MO, USA) for 4-6 hours. Structures containing YFP-immunoreactivity were stained black with a nickel-intensified diaminobenzidine (DAB) reaction in which peroxide was generated using glucose oxidase (Llewellyn-Smith et al., 2005). After a second blocking step in 10% NHS-TBS-Triton, sections were exposed to either 1:5,000 goat anti-ChAT (Catalogue # AB144P, Lot # 18110644 or JC1669317; Chemicon, Temecula, CA, USA), 1:5,000 rabbit anti-TH (Catalogue # AB152, Lot # LV1375881 or LV1532665; Chemicon) or 1:5,000 or 1:10,000 rabbit anti-5-HT (Catalogue #8250-0009, Lot #23073052; Biogenesis, Poole UK) for 2-3 days. Next, there was an overnight incubation in 1:500 biotinylated donkey secondary antibody directed against the immunoglobulin of the species in which the primary antibody was raised, i.e., donkey anti-goat IgG (Catalogue #711-705-065-147; Jackson ImmunoResearch Laboratories Inc.,West Grove, PA, USA) or donkey anti-rabbit IgG (Catalogue #711-065-152; Jackson ImmunoResearch). After a final 4 hour incubation in ExtrAvidin-peroxidase, immunoreactive neurons were stained brown with an imidazole-intensified DAB reaction (Llewellyn-Smith et al., 2005).

2.1.2   *Three-colour Immunoperoxidase Labelling*

Triple immunoperoxidase labelling was used to localise YFP-, TH- and ChAT-immunoreactivity in the same sections. After the two colour protocol was completed using a 1:400,000 dilution of anti-GFP and a 1:5,000 dilution of anti-TH, an additional block with 10% NHS-TBS-Triton was done and the sections were incubated first in 1:5,000 goat anti-ChAT for 2-3 days, then in biotinylated anti-goat IgG overnight and finally in ExtrAvidin-horseradish peroxidise for 4-6 hours. ChAT-immunoreactivity was localised with a Vector SG kit (Vector Laboratories, Burlingame, CA, USA) with reagents added to generate peroxide with glucose oxidase reaction (Llewellyn-Smith et al., 1999).

2.1.3.   *Antibody Characterization*

In our previous study on YFP-PPG mice (Llewellyn-Smith et al., 2011), we demonstrated the specificity of the chicken anti-GFP antiserum used here. We showed that

no staining occurred in sections from animals that lacked GFP-expressing neurons and that the anti-GFP antibody stained all of the neurons that fluoresced due to the presence of YFP.

Sections of rat spinal cord stained with the goat anti-ChAT antiserum show the expected distribution of cholinergic neurons in the spinal cord (Fenwick et al., 2006). When we have used recombinant rat ChAT (Chemicon Catalogue #Ag220) to adsorb this antiserum, we found no staining in tissue fixed and processed as here (Llewellyn-Smith et al., 2005).

The supplier of the rabbit anti-TH antibody has used western blotting to check its specificity and obtained selective labelling of a single band at approximately 62kDa (reduced), which corresponds to TH. In sections from rats perfused and immunohistochemically processed as here using this anti-TH antibody, we have found that the medulla contains immunoreactive neurons with the expected morphologies and distributions and that the spinal cord contains axons with the expected distribution. This antibody has been used extensively to study catecholaminergic innervation in the brain, spinal cord and periphery in a variety of species (e.g. (Cano et al., 2008, Nangle et al., 2009, Gnanamanickam and Llewellyn-Smith, 2011).

We tested the specificity of the anti-5-HT antiserum by adsorbing it with a glutaraldehyde conjugate of 5-HT and keyhole limpet haemocyanin, which we prepared. Adsorbed and unadsorbed antibody solutions were incubated overnight at 4°C and used to immunoperoxidase stain 30 µm cryostat sections of formaldehyde-fixed rat and mouse medulla. Overnight adsorption removed the vast majority of staining but did not completely abolish it. Medulla sections stained with the adsorbed antiserum contained rare, faintly-immunoreactive cell bodies in raphé pallidus and a few immunoreactive axons in the dorsal vagal complex compared to the usual distribution of immunoreactivity obtained with the unabsorbed antiserum.

2.2.   DATA COLLECTION AND ANALYSIS

Immunoperoxidase-stained sections from the spinomedullary junction to the caudal end of the aqueduct were examined with an Olympus BH-2 brightfield microscope. Cell bodies and proximal dendrites containing immunoreactivity for TH, ChAT or serotonin were examined for the presence of close appositions from YFP-positive axon terminals. An x100 oil immersion lens was used to determine whether or not YFP-containing terminals were closely apposed to neurochemically-identified cell bodies and dendrites. YFP terminals lying side-by-side with an immunoreactive neuron were classed as closely apposed when there was no space visible between the terminal and the neuron. In the case of terminals overlying immunoreactive

neurons, a close apposition was considered to be present when the terminal and the filled neuron were in focus in the same plane.

A SPOT RT colour camera and SPOT RT software version 4.6 (Diagnostic Instruments Inc., Sterling Heights, MI, USA) were used to collect digital images from the sections as TIFF files. The sharpness, brightness, and contrast of the TIFFs were adjusted in Adobe PhotoShop, which was also used to colour match digital images. Montages of micrographs and plates containing micrographs were prepared using PhotoShop.

2.2.1   *Mapping neurochemically-identified brainstem neurons that received or lacked YFP-immunoreactive innervation*

To construct line drawings, a SPOT RT colour camera and an x10 objective were used to capture overlapping digital images through the dorsal vagal complex or ventral medulla on one side of the brainstem from each mouse. The micrographs from each section were saved as TIFF files, imported into Adobe Photoshop and montaged to create a single image of the region to be mapped. A layer was added to the montage in PhotoShop and the surface of the medulla was traced with the pen tool. Landmarks were traced with the pen tool on another layer. Low magnification line drawings of each section were created from digital images taken with an x2 objective using a similar strategy.

For recording the distribution of the each different neurochemical class of neuron that received or lacked appositions from YFP-immunoreactive varicosities on the line drawings, a separate layer was added to the TIFF file containing the x10 montage of each section. The position of each neuron was marked with a dot using the pencil tool and a different colour to represent each different type of neuron. To count neurons with and without appositions, the layers with coloured dots were saved as individual TIFF files. Each TIFF file was opened in ImageJ (National Institutes of Health) and the image was converted to black and white. Dots were counted using the Analyze Particle function.

Maps of DMV, AP and A2 neurons: In the dorsal vagal complex from one female mouse, TH-immunoreactive neurons with and without YFP appositions and ChAT-immunoreactive neurons with and without YFP appositions were mapped from every third section triple-stained for YFP, TH and ChAT (60 μm separating mapped sections). A total of 6 sections were mapped. The mapped region included most of the dorsal vagal complex ventral to AP. However, YFP innervation was not assessed in the most caudal portion of the dorsal vagal complex because the dense accumulation of YFP-immunoreactive dendrites

made it impossible to determine whether close appositions were present on TH- or ChAT-immunoreactive neurons.

Maps of A1/C1 neurons: TH-immunoreactive neurons with and without YFP appositions that lay in the A1/C1 column in the ventral medulla from one female mouse were mapped in every sixth section triple-stained for YFP, TH and ChAT (150 μm separating mapped sections). A total of 13 sections were mapped. The mapped region extended from the pyramidal decussation through the caudal portion of the facial nucleus.

Maps of serotonin neurons: Ventral medullary 5-HT neurons with and without appositions from YFP-immunoreactive varicosities were mapped in every sixth section double-stained for YFP and 5-HT from one male mouse (150 μm separating mapped sections).   A total of 8 sections were mapped.   The mapped region extended from approximately the middle of AP to approximately the middle of the facial nucleus.

Plates containing the maps were constructed in Adobe Illustrator. The layer containing the montage was deleted from the TIFF file for each section. The resulting image was imported into Illustrator and the positions of all the neurons were remapped using larger symbols of different colours.

3.   RESULTS

YFP-immunoreactive innervation of catecholamine neurons (Figures 1-4), cholinergic neurons (Figures 1 and 2), and serotonin neurons (Figures 5 and 6) in the brainstem was assessed in 11 adult male and 11 adult female YFP-PPG mice. After immunoperoxidase staining, YFP-PPG neurons in the NTS and IRT showed intense YFP-immunoreactivity throughout their cell bodies and dendrites (Figures 1A-C, I and J). In the brainstem, varicose axons arising from the YFP-PPG neurons were also very intensely stained for YFP. The YFP-containing axons had clearly delineated varicosities and fine intervaricose segments (Figures 1 and 3). Some of the axons had large varicosities; others had small fine varicosities and on some axons both large and small varicosities occurred (e.g., Figures 1G, 1J, 3B). All three types of axons made close appositions on neurochemically-identified brainstems neurons.

The distribution of YFP-expressing neurons in the medulla of YFP-PPG mice was the same as reported previously (Llewellyn-Smith et al., 2011). The largest group of YFP-immunoreactive cell bodies occurred in the caudal lateral NTS and extended caudally from approximately mid-AP level past the caudal tip of AP (Figures 1A, F and I). The second

major group of YFP-immunoreactive somata was located in the IRT, extending from about mid-AP to roughly where the NTS moved away from the fourth ventricle. Triple labelling for GFP, TH and ChAT revealed that the YFP-PPG neurons in IRT lay dorsomedial to both the cholinergic neurons of the nucleus ambiguus (NA) and the noradrenergic neurons of the A1 cell group (Figure 1B).

3.1.   INNERVATION OF CATECHOLAMINE NEURONS BY YFP-IMMUNOREACTIVE PREPROGLUCAGON NEURONS

Catecholamine neurons from the spinomedullary junction to the caudal end of the aqueduct were revealed by immunoreactivity for TH in transverse sections through the brains of 10 male and 7 female YFP-PPG mice (Figures 1 and 3). In the medulla, TH-immunoreactive neurons occurred in the ventrolateral medulla (A1/C1 cell group), the NTS (A2 cell group), the AP and around the midline in the dorsal medulla (C2 and C3 cell groups). In the pons, TH-immunoreactive cell bodies were located around the exit of the facial nerve (A5 cell group) and in the locus coeruleus (A6 cell group).

In the dorsal medulla, some of the TH-immunoreactive neurons of the A2 cell group in the NTS received close appositions from YFP-immunoreactive axons (Figures 1C-E and 2). These appositions were more common in the region where YFP-immunoreactive cell bodies and dendrites formed a dense network throughout the NTS (Figure 2). In AP, a small number of TH-immunoreactive cells were closely apposed by YFP-immunoreactive axons (Figures 1F-H and 2). There were fewer TH-positive neurons with appositions in caudal AP than in rostral AP (Figure 2). Throughout AP, the TH-containing neurons that received close appositions usually occurred near the lateral edge of AP or within the clusters of TH-positive neurons that lay on the dorsal surface of the most rostral portion of AP (Figure 2). TH-positive C2 and C3 neurons near the dorsal medullary midline received little YFP-positive innervation (not shown).

As we have described previously, there was a moderate YFP-immunoreactive innervation of the rostral ventrolateral medulla (RVLM). Boutons of YFP-positive axons in this region closely apposed the somata or proximal dendrites of some TH-immunoreactive C1 neurons (Figures 3A-C and 4). Close appositions from YFP-immunoreactive axons also occurred on TH-positive neurons of the A1 cell group in the caudal ventrolateral medulla (Figure 4). Although rare on the most caudal A1 neurons near the spinomedullary junction (not shown), appositions from YFP-positive axons were common on TH-immunoreactive A1

neurons in the intermediate reticular region ventral to AP (Figure 4). Near the caudal tip of the 4th ventricle, TH-positive neurons in the rostroventral respiratory group also received close appositions from YFP-immunoreactive axons.

In the ventral pons, YFP-immunoreactive varicosities closely apposed the somata or proximal dendrites of occasional TH-immunoreactive neurons of the A5 cell group. In the dorsal pons, TH-immunoreactive A6 neurons of the locus coeruleus formed a dense band of cell bodies (Figure 3D-F). Few YFP-immunoreactive axons penetrated the locus coeruleus region and the cell bodies of TH-positive A6 neurons only rarely received close appositions from YFP-positive boutons (Figure 3E, F). Many more varicose YFP-positive axons occurred within the neighbouring and more medially located Barrington's nucleus (Figure 3E). The TH-positive dendrites of A6 neurons penetrated the more heavily innervated area of Barrington's nucleus but close appositions by YFP-immunoreactive varicosities were still rare on the dendrites that originated from the A6 neurons in locus coeruleus.

In all of the TH-immunoreactive cell groups examined, innervated neurons generally received close appositions from 1-3 varicosities on a single YFP-immunoreactive axon.

3.2.   *PREPROGLUCAGON INNERVATION OF CHOLINERGIC NEURONS*

Cholinergic neurons were revealed by the presence of ChAT-immunoreactivity in their cytoplasm. Transverse sections between the spinomedullary junction and the caudal end of the aqueduct were analysed from 4 male and 9 female YFP-PPG mice. These sections contained major cholinergic cell populations in the hypoglossal nucleus, the dorsal motor nucleus of the vagus (DMV), NA, the facial nucleus and the abducens, pedunculopontine and tegmental nuclei.

A relatively small proportion of the ChAT-immunoreactive DMV neurons were directly innervated by axons containing immunoreactivity for YFP (Figures 1I and J, 2). Near the spinomedullary junction, the DMV contained a moderate supply of varicose YFP-immunoreactive axons. Nevertheless, at this most caudal level of the DMV, only occasional ChAT-positive dorsal vagal motor neurons received close appositions. PPG cell bodies marked by YFP-immunoreactivity were located more rostrally in the NTS beneath AP (see above). At this level, a dense network of YFP-positive dendrites was present along the ventral aspect of the DMV. More DMV neurons in this region than rostrally or caudally appeared to receive close appositions from YFP-positive terminals but the network of YFP-PPG dendrites may also have obscured some appositions. Mapping ChAT-positive DMV

neurons with and without appositions from YFP-immunoreactive varicosities ventral to AP (Figure 2) showed that motor neurons receiving GLP-1 innervation were distributed throughout the subpostremal DMV. Nevertheless, innervated neurons were most often encountered medially and ventrally in this portion of the nucleus. Occasional DMV neurons rostral to AP were also closely apposed by YFP-containing terminals. In sections triple-stained for YFP, TH and ChAT, YFP-immunoreactive appositions were present on a very small number of DMV neurons containing immunoreactivity for both ChAT and TH (not shown). When DMV neurons were innervated, it was usually by a single YFP-immunoreactive axon that had 1-3 fine, small varicosities in close apposition to the ChAT-positive neuron (Figure 1J).

In contrast to the DMV, very few YFP-immunoreactive axons travelled through the hypoglossal nucleus and none closely apposed ChAT-positive hypoglossal motor neurons. A small population of neurons with faint ChAT-immunoreactivity was located ventral to the rostral NA close to the surface of the medulla. YFP-immunoreactive axons with fine varicosities made rare close appositions on these ventral cholinergic neurons. Although YFP-containing axons ran amongst the cholinergic neurons of the loose portion of NA, no close appositions were found. The compact formation of NA was also virtually devoid of YFP-immunoreactive axons.

Few YFP-immunoreactive axons occurred in the facial nucleus. Close appositions were almost never encountered on ChAT-positive neurons in this region. The rare neurons that did receive YFP-immunoreactive input were mostly located in the most medial part of the facial nucleus. Similarly, the nucleus abducens was virtually devoid of YFP-immunoreactive axons and close appositions were never found. Further rostral, cholinergic neurons in the trigeminal motor nucleus did not receive a YFP-positive innervation although YFP-containing axons traversed the lateral edge of the nucleus. However, rare ChAT-positive neurons of the laterodorsal tegmental nucleus received close appositions from YFP-immunoreactive axons. Single close appositions from YFP-positive varicosities also occurred on the somata or proximal dendrites of occasional pedunculopontine tegmental neurons.

3.3. *PREPROGLUCAGON INNERVATION OF SEROTONIN NEURONS*

5-HT-immunoreactive neurons from the spinomedullary junction to the decussation of the superior cerebellar peduncle were revealed in transverse sections from 5 male and 5 female YFP-PPG mice. The most caudal 5-HT-immunoreactive cell bodies were located in

raphé pallidus, raphé obscurus, the parapyramidal region (PPY) and along the ventral surface of the medulla (Figures 5 and 6). The 5-HT-immunoreactive neurons on the ventral surface first appeared in the region of AP (beneath caudal AP in some mice and beneath rostral AP in others) and disappeared at about the level of the rostral edge of NA. The 5-HT-positive PPY neurons were located just lateral to the pyramids and were roughly co-extensive rostrocaudally with the motor neurons of NA. The long axes of many of the serotonergic PPY cell bodies were oriented dorsoventrally (Figure 5B). At the level of the caudal facial nucleus, the dorsoventrally-oriented cell bodies characteristic of PPY serotonin neurons transitioned into cell bodies with a predominantly mediolateral orientation, which were the serotonin neurons of raphé magnus. The dorsal raphé and pontine raphé nuclei contained the most rostral 5-HT-immunoreactive neurons examined.

The serotonin-containing neurons in PPY and on the ventral medullary surface were the most densely innervated of any of the neurochemically-identified neurons in this study (Figures 5B, D, E and 6). The cell bodies and proximal dendrites of almost all of these neurons received several close appositions from YFP-positive terminals. In general, close appositions from YFP-immunoreactive axons were somewhat less common on neurons in raphé pallidus than on PPY neurons. However, for both raphé pallidus neurons and PPY neurons, the density of appositions was highest at the caudal end of their distributions and diminished rostrally (Figure 6).

YFP-immunoreactive axons also travelled through raphé magnus and the dorsal and pontine raphé nuclei. In all of these locations, occasional 5-HT-immunoreactive neurons received close apposition from YFP-labelled varicosities but the majority of serotonin neurons in these locations did not receive YFP innervation.

Overall, more 5-HT-immunoreactive neurons in the medulla were innervated than were cholinergic or catecholamine neurons and the majority of caudal medullary 5-HT-positive neurons received close appositions from YFP-immunoreactive varicosities. The YFP innervation of individual serotonin neurons was also denser than the innervation of individual cholinergic or catecholamine neurons. Each innervated ChAT-positive or TH-positive neuron received between one and three close appositions from YFP-containing varicosities. In contrast, 5-HT-immunoreactive somata in the caudal medulla often received at least twice this number of appositions.

4.   DISCUSSION

In this study, we used two- and three-colour immunoperoxidase labelling to assess the GLP-1 innervation of neurochemically-identified brainstem neurons in YFP-PPG mice (Reimann et al., 2008, Llewellyn-Smith et al., 2011). YFP expression in these mice is restricted to cells in which the PPG promoter is active (Reimann et al., 2008, Hisadome et al., 2010). Consequently, in these mice, YFP-immunoreactivity occurs exclusively in cells that synthesize PPG, the precursor for glucagon, as well as GLP-1, GLP-2 and oxyntomodulin (Holst, 2007). As a result, YFP labels only pancreatic α-cells that produce glucagon, enteroendocrine L-cells and populations of central neurons that produce GLP-1 and GLP-2 in equimolar amounts (Reimann et al., 2008). Single-cell RT-PCR has demonstrated that the YFP-expressing cells in YFP-PPG mice still produce PPG mRNA and should therefore synthesize GLP-1 in addition to YFP (Hisadome et al., 2010, 2011). Here, in addition to revealing YFP, we visualized neurons releasing catecholamines or acetylcholine using the presence of immunoreactivity for enzymes involved in the synthesis of these neurotransmitters (TH and ChAT, respectively). Immunoreactivity for 5-HT was used to identify serotonin neurons. We assumed that YFP-containing axon terminals found in close apposition to TH-, ChAT- or 5-HT-immunoreactive cell bodies or dendrites signified innervation. Whilst only electron microscopy can provide the ultimate proof for this assumption, work on other types of central autonomic neurons has shown that at least half of the terminals that form close appositions at the light microscope level make synaptic contacts at the ultrastructural level (Pilowsky et al., 1992).

Of brainstem neurons containing immunoreactivity for TH, 5-HT or ChAT, serotonin neurons received the heaviest YFP innervation. A high proportion of the 5-HT-positive neurons in the parapyramidal region and on the ventral surface of the medulla received many close appositions from YFP-immunoreactive varicosities. Appositions were also common on serotonin neurons in raphé pallidus and occurred on some neurons in caudal raphé obscurus. In contrast, neurons in raphé magnus and the dorsal raphé nuclei were moderately to sparsely innervated. Amongst brainstem catecholamine neurons, a significant fraction of the TH-immunoreactive neurons in the A1/C1 column in the ventrolateral medulla received close appositions, with 1-3 varicosities on the same axon providing innervation to a soma or proximal dendrite. In contrast, only rare TH-immunoreactive neurons in the locus coeruleus received appositions from YFP-positive varicosities. Of brainstem cholinergic neurons, only a subset of ChAT-positive neurons in the DMV received appositions from

YFP-containing axons. A small number of DMV cell bodies with appositions also contained immunoreactivity for TH. Cholinergic DMV neurons with appositions most commonly occurred at the same rostrocaudal level as the cell bodies and dendrites of YFP-PPG neurons. The remaining groups of brainstem cholinergic neurons, including those in NA and the hypoglossal nucleus, essentially lacked YFP innervation. All of the neuronal populations mentioned above as receiving close appositions from YFP-immunoreactive varicosities have been shown to express mRNA for the GLP-1 receptor (Merchenthaler et al., 1999).

4.1.   INNERVATION OF AREA POSTREMA

Activation of GLP-1 receptors within the brainstem is associated with a number of physiological and pathophysiological effects. Pharmacological activation of GLP-1 receptors in the brainstem reduces gut motility (Holmes et al., 2009), mediates lipopolysaccharide-induced anorexia (Grill et al., 2004), influences satiety elicited by gastric distension (Hayes et al., 2009) and causes hypothermia (Skibicka et al., 2009). In AP, GLP-1 receptors reside primarily on catecholamine neurons (Goke et al., 1995, Merchenthaler et al., 1999), which exhibit Fos-immunoreactivity after intravenous administration of the GLP-1 receptor agonist exendin-4 (Yamamoto et al., 2002, Yamamoto et al., 2003). Because the AP has an incomplete blood-brain-barrier, it has been suggested that these receptors are a 'gateway' through which GLP-1 from the circulation can influence central nervous function. However, our previous study demonstrated that YFP-PPG neurons send axons into AP (Llewellyn-Smith et al., 2011) and we suggested that GLP-1 released from these axons, rather than circulating GLP-1, might activate at least some of the receptors in AP. Indeed, our present results demonstrate that YFP-PPG neurons innervate catecholaminergic AP neurons although this innervation is relatively sparse. It is therefore possible that both centrally-derived and peripherally-produced GLP-1 might activate receptors within AP.

4.2.   GASTRIC AND PANCREATIC FUNCTION

Neurons in the DMV respond functionally to GLP-1 or its stable analogue exendin-4. *In vivo*, activation of GLP-1 receptors in the DMV has been linked to a reduction in gut motility (Holmes et al., 2009). *In vitro,* both gastric-projecting and pancreas-projecting dorsal vagal motor neurons alter their electrical activity in response to GLP-1 application (Wan et al., 2007a, Wan et al., 2007b, Holmes et al., 2009). In the presence of TTX, about 40% of pancreas-projecting DMV neurons maintained their GLP-1 induced depolarisation,

and thus are expected to have GLP-1 receptors (Wan et al., 2007b). In agreement with these pharmacological data, we found that a subset of ChAT-immunoreactive neurons within the DMV had a sparse YFP-immunoreactive innervation. Interestingly, DMV neurons with YFP-positive appositions often occurred near the medial portion of the nucleus, where we have previously identified neurons that express Fos in response to glucoprivation induced by 2-deoxyglucose in rats (Llewellyn-Smith et al., 2012) Furthermore, in rats, DMV neurons containing both TH- and ChAT-immunoreactivity project exclusively to the gastric corpus (Guo et al., 2001). In this study, we found that a very small number of DMV neurons with this neurochemistry received YFP-positive innervation. Despite these observations, tracing experiments will be required to determine whether the DMV innervation reported here specifically targets gastric- and pancreas-projecting neurons or neurons supplying other regions of the gastrointestinal tract or other organs. At the level of the DMV, GLP-1 appears to be excitatory (Wan et al., 2007b, Holmes et al., 2009). However, its effect on gastric motility is inhibitory, suggesting that non-adrenergic, non-cholinergic vagal postganglionic neurons are part of the circuitry that mediates the effects of GLP-1 at the level of the stomach (Travagli et al., 2006, Holmes et al., 2009).

4.3.   CARDIOVASCULAR CONTROL

In this study, we found that YFP-PPG neurons innervated ventral medullopontine catecholamine cell groups, including A1, A5 and C1 neurons. We found substantial numbers of YFP-positive axons throughout the rostrocaudal extent of the ventrolateral medulla and catecholaminergic A1 and C1 neurons clearly received close appositions. C1 neurons of the RVLM are important for regulation of blood pressure because they mediate sympathetic tone (Abbott et al., 2009, Marina et al., 2011, Schreihofer and Sved, 2011). It seems feasible to assume that the innervation of C1 neurons described here provides an anatomical substrate for at least some of the demonstrated cardiovascular effects of central GLP-1 administration (Yamamoto et al., 2002, Cabou et al., 2008, Hayes et al., 2008). Since catecholamine neurons in the A1 region project to the hypothalamus (Sawchenko and Swanson, 1982, Rinaman, 2001), GLP-1 inputs to A1 neurons could influence cardiovascular homeostasis as well as other autonomic functions through an A1-hypothalamus pathway. We also found that A5 catecholamine neurons received input from YFP-immunoreactive axons. GLP-1 input to A5 neurons may also influence sympathetic control of blood pressure (Guyenet, 2006). In contrast to the C1, A1 and A5 neurons, catecholaminergic A6 neurons of the locus coeruleus

in the dorsal pons were almost completely without innervation from YFP-immunoreactive axons. This observation suggests that any influence of central GLP-1 on wakefulness and arousal (Sara, 2009) is unlikely to be mediated by locus coeruleus neurons.

The innervation of Barrington's nucleus by YFP-immunoreactive axons could have significance for the control of autonomic function. This nucleus is important for the control of micturition (Sasaki, 2005) and viral tracing studies have shown that Barrington's nucleus is also part of the circuitry that controls sympathetically innervated targets such as the kidney, spleen and brown adipose tissue (Cano et al., 2000, Cano et al., 2003).

4.4.   *AUTONOMIC FUNCTIONS CONTROLLED BY SEROTONIN NEURONS*

We found here that GLP-1 axons heavily innervated the majority of 5-HT neurons in ventral regions of the medulla and also provided input to other serotonergic nuclei in the brainstem. Serotonin (5-HT) is important for the control of a variety of homeostatic processes, including energy balance, respiration and body temperature (Breisch et al., 1976, Ray et al., 2011).

The strong innervation of 5-HT neurons in the ventral medulla might play an important role in the satiating effects of central GLP-1. GLP-1 and 5-HT have both been implicated in the regulation of food intake (Tang-Christensen et al., 1996, Turton et al., 1996, Halford et al., 2010, Lam et al., 2010). A role of 5-HT downstream of GLP-1 is suggested by the finding that 5-HT-receptor 2C knockout mice fail to show satiation after intraperitoneal administration of GLP-1 (Asarian, 2009). Anorexia caused by lipopolysaccharide (LPS) is also likely to involve both GLP-1 signalling and 5-HT receptors (Langhans, 2007). LPS induces Fos-immunoreactivity in both GLP-1 neurons in the NTS (Rinaman, 1999) and in serotonin neurons of raphé pallidus, raphé magnus and dorsal and median raphé nuclei (Kopf et al., 2010). Furthermore, both injection of the GLP-1 antagonist exendin-9 into the 4th ventricle (Grill et al., 2004) and intraperitoneal administration of the brain-penetrant serotonin 2C-receptor antagonist SB 242084 reduce anorexia evoked by LPS (Kopf et al., 2010). Taken together with our observation that 5-HT immunoreactive neurons in raphé nuclei receive close appositions from the axons of GLP-1 neurons, these data might indicate that 5-HT neurons are also a downstream target of GLP-1 neurons involved in LPS-induced anorexia.

GLP-1 might also affect thermoregulatory responses through an input to 5-HT neurons. Pharmacogenetic suppression of electrical activity in serotonin neurons *in vivo*

causes hypothermia and a reduction in respiratory chemosensitivity (Ray et al., 2011). The effects of central GLP-1 on chemosensitivity have not been assessed, but activation of brainstem GLP-1 receptors has been shown to cause hypothermia (Hayes et al., 2008). Furthermore, blockade of hindbrain GLP-1 receptor with exendin-9 prevents CART-induced hypothermia (Skibicka et al., 2009). Innervation of raphé pallidus neurons could provide a link between central GLP-1 and thermogenesis, as 5-HT neurons in this region are known to stimulate neurons in sympathetic nuclei of the spinal cord, which in turn promote brown adipose tissue metabolism (Morrison et al., 2008). As the GLP-1 receptor is predominantly coupled to G_s (Thorens and Widmann, 1996), it remains to be determined if raphé pallidus neurons are inhibited by GLP-1 or if the hypothermic effects of central GLP-1 involve alternative neuronal circuits.

4.5. *CONCLUSIONS*

In summary, this study provides the first detailed description of the GLP-1 innervation of neurochemically-identified monoamine and serotonin neurons in the brainstem. Our observations create an anatomical scaffold for understanding the diverse array of autonomic functions affected by central GLP-1. We expect that the information about the distribution of GLP-1 inputs to brainstem neurons presented here will provide a valuable guide for functional studies probing the roles of central GLP-1 neurons.

FIGURE LEGENDS (ONLINE VERSION)

FIGURE 1.   Three-colour immunoperoxidase labelling for YFP in YFP-PPG neurons (black), tyrosine hydroxylase (TH) in catecholamine neurons (brown) and choline acetyltransferase (ChAT) in cholinergic neurons (blue-grey) in transverse sections through the dorsal medulla of YFP-PPG mice. **A**, Low magnification micrograph showing the cell bodies of black, YFP-immunoreactive PPG neurons in the nucleus of the solitary tract (NTS). These neurons lie lateral to the dorsal motor nucleus of the vagus (DMV) and the majority occur at the level of the area postrema (AP). The dendrites of the YFP-PPG neurons in NTS extend dorsomedially and also run lateral to the hypoglossal nucleus (HGN) and along the border between the DMV and the HGN. cc, central canal. Bar, 100 µm. **B**, In the intermediate reticular nucleus (IRT), the black, YFP-immunoreactive cell bodies of PPG neurons are located dorsomedial to both the brown, TH-immunoreactive neurons of the A1 cell group and the blue-grey, ChAT-immunoreactive neurons of the nucleus ambiguus (NA). Bar, 100 µm. **C**, Low magnification micrograph showing the dorsal vagal complex at the level of the most rostral YFP-PPG neurons. A collection of YFP-immunoreactive dendrites travels between the DMV and HGN. Arrows, brown, TH-immunoreactive cell bodies that are shown at higher magnification in D and E. Bar, 250 µm. **D and E,** Single varicosities (arrows) of black, YFP-immunoreactive axons closely appose brown, TH-immunoreactive cell bodies in the NTS. Bars, 20 µm. **F**, Low magnification micrograph showing the AP near the level of the most rostral YFP-PPG neurons. Arrow, a brown, TH-immunoreactive cell body near the surface of AP that is shown at higher magnification in G. Bar, 100 µm. **G,** A single varicosity (arrow) of a black, YFP-immunoreactive axon closely apposes the brown, TH-immunoreactive cell body in AP. Bar, 10 µm. **H**, At the surface of rostral AP, black, varicose, YFP-immunoreactive axons and black, varicose, YFP-immunoreactive dendrites are intermixed with brown, TH-immunoreactive dendrites arising from AP neurons. Bar, 20 µm. **I**, Low magnification micrograph showing the DMV near the level of the most rostral YFP-PPG neurons. Arrows J1 and J2, two blue-grey, ChAT-immunoreactive vagal motor neurons that are shown at higher magnification in J. Bar, 100 µm. **J,** Fine varicosities (arrows) of black, YFP-immunoreactive axons closely appose the blue-grey, ChAT-immunoreactive cell bodies of DMV neurons J1 and J2. Bar, 20 µm.

FIGURE 2.   Maps of sections through the dorsal vagal complex of a YFP-PPG mouse showing the distribution of ChAT-immunoreactive and TH-immunoreactive neurons with and without close appositions from YFP-immunoreactive varicosities. Sections were triple-stained to reveal YFP, TH and ChAT. Every third section was mapped; maps are therefore separated by 60μm. The most caudal section is at the top left of the figure and the most rostral section is at the bottom right. TH-immunoreactive neurons in the nucleus tractus solitarius (NTS) and area postrema (AP) are represented by circles; and ChAT-immunoreactive neurons, predominantly in the dorsal motor nucleus of the vagus (DMV), by diamonds.   TH-immunoreactive neurons that receive close appositions from YFP-immunoreactive varicosities are shown in red; those that do not receive appositions are shown in blue. ChAT-immunoreactive neurons that receive close appositions from YFP-immunoreactive varicosities are shown in gold; those that do not receive appositions are shown in green.   The cell bodies of YFP-PPG neurons are represented by white stars. Numerical values indicate the proportion of neurons in each region that received close appositions from YFP-immunoreactive varicosities.   The percentages of neurons that received YFP- immunoreactive appositions in each region are given in parentheses.   The asterisk indicates an area of the DMV in which appositions could not be assessed because the dendrites of YFP-PPG neurons were too dense. cc, central canal; HGN, hypoglossal nucleus.

FIGURE 3.   Two-colour immunoperoxidase labelling for YFP in YFP-PPG neurons (black) and tyrosine hydroxylase (TH) in catecholamine neurons (brown) in transverse sections through the rostral ventrolateral medulla (RVLM) and dorsal pons of YFP-PPG mice.   **A,** Low magnification micrograph showing the RVLM. Arrows, brown, TH-immunoreactive cell bodies that are shown at higher magnification in D and E. py, pyramidal tract. Bar, 100 μm. **B and C,** Single varicosities (arrows) of black, YFP-immunoreactive axons closely appose brown, TH-immunoreactive cell bodies in the RVLM. Bar in B, 10 μm; bar in C, 20 μm. **D**, Low magnification micrograph showing the region of the locus coeruleus (LC) and Barrington's nucleus (Bar). Left is medial and the ventricle appears at top left. The region in Box E is shown at higher magnification in E. Arrow F, a brown, TH-immunoreactive neuron in the subcoeruleus region (SubC) that is shown at higher magnification in F. Bar, 250 μm. **E,** There are many black, varicose YFP-immunoreactive axons in Bar. However, only a few, black, varicose YFP-immunoreactive axons travel amongst the brown, TH-immunoreactive neurons of LC. Of all of the TH-immunoreactive cell bodies in this region of LC, only 6 received close appositions from YFP-immunoreactive

varicosities, one of which (lower right) is marked by an arrowhead. There were no close appositions on the TH-immunoreactive dendrites of LC neurons that penetrated Bar. Bar, 50 μm. **F**, A single varicosity (arrow) of a black, YFP-immunoreactive axon closely apposes the brown, TH-immunoreactive cell body in SubC. Bar, 20 μm.

FIGURE 4.   Maps of sections through the ventral medulla of a YFP-PPG mouse showing the distribution of TH-immunoreactive neurons with and without close appositions from YFP-immunoreactive varicosities.   Sections were triple-stained to reveal YFP, TH and ChAT. Every sixth section was mapped; maps are therefore separated by 150μm. The most caudal section is at the top left of the figure and the most rostral section is at the bottom right. TH-immunoreactive neurons that receive close appositions from YFP-immunoreactive varicosities are represented by red circles; TH-immunoreactive neurons that do not receive appositions are represented by blue circles.   The cell bodies of YFP-PPG neurons are represented by white stars.   Numerical values indicate the proportion of neurons in each section that received close appositions from YFP-immunoreactive varicosities.   The percentages of neurons that received YFP- immunoreactive appositions in each section are given in parentheses.   The insets show the entire section from which each map was constructed, allowing the dorsoventral tilt of the section can be assessed. FN, facial nucleus; IO, inferior olive; NAc, compact formation of the nucleus ambiguus; py, pyramidal tract; pyx, pyramidal decussation.

FIGURE 5.   Two-colour immunoperoxidase labelling for YFP in YFP-PPG neurons (black) and 5-HT in serotonin neurons (brown) in transverse sections through the caudal ventral medulla of YFP-PPG mice. **A**, Low magnification micrograph showing the ventral medulla from the midline through the RVLM, Arrows B and C, brown, groups of 5-HT-immunoreactive cell bodies that are shown at higher magnification in B and C. py, pyramidal tract.   Bar, 100 μm. **B,** In the parapyramidal region (PPY), a cluster of serotonin-immunoreactive cells bodies receives close appositions from many YFP-immunoreactive axons. Bar, 20 μm. **C,** The cell bodies of two brown, 5-HT immunoreactive neurons in raphé pallidus (RPa) receive several close apposition from varicosities (arrows) of black, YFP-immunoreactive axons. Bar, 10 μm. **D**, A black, YFP-immunoreactive varicosity (arrow) forms a close apposition on a brown, 5-HT immunoreactive cell body that lies near the ventral surface (VS) in PPY. Bar, 10 μm. **E**, Two black varicosities on the same YFP-

immunoreactive axon (arrows) closely appose a brown, 5-HT-immunoreactive cell body in RPa. Bar, 10 µm.

FIGURE 6.   Maps of sections through the ventral medulla of a YFP-PPG mouse showing the distribution of 5-HT-immunoreactive neurons with and without close appositions from YFP-immunoreactive varicosities. Sections were double-stained to reveal YFP and 5-HT. Every sixth section was mapped; maps are therefore separated by 150µm. The most caudal section is at the top left of the figure and the most rostral section is at the bottom right. 5-HT-immunoreactive neurons that receive close appositions from YFP-immunoreactive varicosities are represented by red circles; 5-HT-immunoreactive neurons that do not receive appositions are represented by blue circles. The cell bodies of YFP-PPG neurons are represented by white stars. Numerical values indicate the proportion of 5-HT-immunoreactive neurons in different region or the entire mapped population that received close appositions from YFP-immunoreactive varicosities. The percentages of neurons that received YFP-immunoreactive appositions are given in parentheses. The insets show the entire section from which each map was constructed, allowing the dorsoventral tilt of the section to be assessed. FN, facial nucleus; IO, inferior olive; NAc, compact formation of the nucleus ambiguus; py, pyramidal tract; RPa, raphé pallidus; VS, ventral surface..

FIGURE LEGENDS (PRINT VERSION)

*FIGURE 1.   Three-colour immunoperoxidase labelling for YFP in YFP-PPG neurons (black), tyrosine hydroxylase (TH) in catecholamine neurons (brown) and choline acetyltransferase (ChAT) in cholinergic neurons (blue-grey) in transverse sections through the dorsal medulla of YFP-PPG mice. **A,** Low magnification micrograph showing the cell bodies of black, YFP-immunoreactive PPG neurons in the nucleus of the solitary tract (NTS). These neurons lie lateral to the dorsal motor nucleus of the vagus (DMV) and the majority occur at the level of the area postrema (AP). The dendrites of the YFP-PPG neurons in NTS extend dorsomedially and also run lateral to the hypoglossal nucleus (HGN) and along the border between the DMV and the HGN. cc, central canal. Bar, 100 µm. **B,** In the intermediate reticular nucleus (IRT), the black, YFP-immunoreactive cell bodies of PPG neurons are located dorsomedial to both the brown, TH-immunoreactive neurons of the A1*

*cell group and the blue-grey, ChAT-immunoreactive neurons of the nucleus ambiguus (NA). Bar, 100 µm. **C**, Low magnification micrograph showing the dorsal vagal complex at the level of the most rostral YFP-PPG neurons. A collection of YFP-immunoreactive dendrites travels between the DMV and HGN. Arrows, brown, TH-immunoreactive cell bodies that are shown at higher magnification in D and E. Bar, 250 µm. **D and E,** Single varicosities (arrows) of black, YFP-immunoreactive axons closely appose brown, TH-immunoreactive cell bodies in the NTS. Bars, 20 µm. **F**, Low magnification micrograph showing the AP near the level of the most rostral YFP-PPG neurons. Arrow, a brown, TH-immunoreactive cell body near the surface of AP that is shown at higher magnification in G. Bar, 100 µm. **G,** A single varicosity (arrow) of a black, YFP-immunoreactive axon closely apposes the brown, TH-immunoreactive cell body in AP. Bar, 10 µm. **H**, At the surface of rostral AP, black, varicose, YFP-immunoreactive axons and black, varicose, YFP-immunoreactive dendrites are intermixed with brown, TH-immunoreactive dendrites arising from AP neurons. Bar, 20 µm. **I**, Low magnification micrograph showing the DMV near the level of the most rostral YFP-PPG neurons. Arrows J1 and J2, two blue-grey, ChAT-immunoreactive vagal motor neurons that are shown at higher magnification in J. Bar, 100 µm. **J,** Fine varicosities (arrows) of black, YFP-immunoreactive axons closely appose the blue-grey, ChAT-immunoreactive cell bodies of DMV neurons J1 and J2. Bar, 20 µm.*

__FIGURE 2.__   Maps of sections through the dorsal vagal complex of a female YFP-PPG mouse showing the distribution of ChAT-immunoreactive and TH-immunoreactive neurons with and without close appositions from YFP-immunoreactive varicosities. Sections were triple-stained to reveal YFP, TH and ChAT. Every third section was mapped; maps are therefore separated by 60µm. The most caudal section is at the top left of the figure and the most rostral section is at the bottom right. TH-immunoreactive neurons in the nucleus tractus solitarius (NTS) and area postrema (AP) that receive close appositions from YFP-immunoreactive varicosities are represented by black circles; TH-immunoreactive neurons that do not receive appositions are represented by grey circles. ChAT-immunoreactive neurons, predominantly in the dorsal motor nucleus of the vagus (DMV), that receive close appositions from YFP-immunoreactive varicosities are represented by black diamonds with white centres; ChAT-immunoreactive neurons that do not receive appositions are represented by pale grey diamonds. The cell bodies of YFP-PPG neurons are represented by white stars. Numerical values indicate the proportion of neurons in each region that received close appositions from YFP-immunoreactive varicosities. The percentages of neurons that

received YFP- immunoreactive appositions in each region are given in parentheses. The asterisk indicates an area of the DMV in which appositions could not be assessed because the dendrites of YFP-PPG neurons were too dense. cc, central canal; HGN, hypoglossal nucleus.

FIGURE 3.   *Two-colour immunoperoxidase labelling for YFP in YFP-PPG neurons and tyrosine hydroxylase (TH) in catecholamine neurons in transverse sections through the rostral ventrolateral medulla (RVLM) and dorsal pons of YFP-PPG mice. **A**, Low magnification micrograph showing the RVLM. Arrows, TH-immunoreactive cell bodies that are shown at higher magnification in D and E. py, pyramidal tract. Bar, 100 μm. **B and C,** Single varicosities (arrows) of black, YFP-immunoreactive axons closely appose TH-immunoreactive cell bodies in the RVLM. Bar in B, 10 μm; bar in C, 20 μm. **D**, Low magnification micrograph showing the region of the locus coeruleus (LC) and Barrington's nucleus (Bar). Left is medial and the ventricle appears at top left. The region in Box E is shown at higher magnification in E. Arrow F, a TH-immunoreactive neuron in the subcoeruleus region (SubC) that is shown at higher magnification in F. Bar, 250 μm. **E**, There are many black, varicose YFP-immunoreactive axons in Bar. However, only a few, black, varicose YFP-immunoreactive axons travel amongst the TH-immunoreactive neurons of LC. Of all of the TH-immunoreactive cell bodies in this regions of LC, only 6 received close appositions from YFP-immunoreactive varicosities, one of which (lower right) is marked by an arrowhead. There were no close appositions on the TH-immunoreactive dendrites of LC neurons that penetrated Bar. Bar, 50 μm. **F**, A single varicosity (arrow) of a black, YFP-immunoreactive axon closely apposes a TH-immunoreactive cell body in SubC. Bar, 20 μm.*

FIGURE 4.   *Maps of sections through the ventral medulla of a female YFP-PPG mouse showing the distribution of TH-immunoreactive neurons with and without close appositions from YFP-immunoreactive varicosities. Sections were triple-stained to reveal YFP, TH and ChAT. Every sixth section was mapped; maps are therefore separated by 150μm. The most caudal section is at the top left of the figure and the most rostral section is at the bottom right. TH-immunoreactive neurons that receive close appositions from YFP-immunoreactive varicosities are represented by black circles; TH-immunoreactive neurons that do not receive appositions are represented by grey circles. The cell bodies of YFP-PPG neurons are represented by white stars. Numerical values indicate the proportion of neurons in each*

section that received close appositions from YFP-immunoreactive varicosities. The percentages of neurons that received YFP- immunoreactive appositions in each section are given in parentheses. The insets show the entire section from which each map was constructed so that the dorsoventral tilt of the section can be assessed. FN, facial nucleus; IO, inferior olive; NAc, compact formation of the nucleus ambiguus; py, pyramidal tract; pyx, pyramidal decussation.

FIGURE 5. *Two-colour immunoperoxidase labelling for YFP in YFP-PPG neurons and 5-HT in serotonin neurons in transverse sections through the caudal ventral medulla of YFP-PPG mice. **A**, Low magnification micrograph showing the ventral medulla from the midline through the RVLM, Arrows B and C, groups of 5-HT-immunoreactive cell bodies that are shown at higher magnification in B and C. py, pyramidal tract. Bar, 100 μm. **B,** In the parapyramidal region (PPY), a cluster of 5-HT-immunoreactive cells bodies receives close appositions from many YFP-immunoreactive axons. Bar, 20 μm. **C,** The cell bodies of two 5-HT immunoreactive neurons in raphé pallidus (RPa) receive several close apposition from varicosities (arrows) of black, YFP-immunoreactive axons. Bar, 10 μm. **D**, A black, YFP-immunoreactive varicosity (arrow) forms a close apposition on a 5-HT immunoreactive cell body that lies near the ventral surface (VS) in PPY. Bar, 10 μm. **E**, Two black varicosities on the same YFP-immunoreactive axon (arrows) closely appose a 5-HT-immunoreactive cell body in RPa. Bar, 10 μm.*

FIGURE 6. *Maps of sections through the ventral medulla of a male YFP-PPG mouse showing the distribution of 5-HT-immunoreactive neurons with and without close appositions from YFP-immunoreactive varicosities. Sections were double-stained to reveal YFP and 5-HT. Every sixth section was mapped; maps are therefore separated by 150μm. The most caudal section is at the top left of the figure and the most rostral section is at the bottom right. 5-HT-immunoreactive neurons that receive close appositions from YFP-immunoreactive varicosities are represented by black circles; 5-HT-immunoreactive neurons that do not receive appositions are represented by grey circles. The cell bodies of YFP-PPG neurons are represented by white stars. Numerical values indicate the proportion of 5-HT-immunoreactive neurons in different region or the entire mapped population that received close appositions from YFP-immunoreactive varicosities. The percentages of neurons that received YFP-immunoreactive appositions are given in parentheses. The insets show the entire section from which each map was constructed so that the dorsoventral tilt of the*

section can be assessed. FN, facial nucleus; IO, inferior olive; NAc, compact formation of the nucleus ambiguus; py, pyramidal tract; RPa, raphé pallidus; VS, ventral surface.

LITERATURE CITED

Abbott SB, Stornetta RL, Socolovsky CS, West GH, Guyenet PG (2009) Photostimulation of channelrhodopsin-2 expressing ventrolateral medullary neurons increases sympathetic nerve activity and blood pressure in rats. J Physiol 587:5613-5631.

Asarian L (2009) Loss of cholecystokinin and glucagon-like peptide-1-induced satiation in mice lacking serotonin 2C receptors. Am J Physiol Regul Integr Comp Physiol 296:R51-56.

Barrera JG, Jones KR, Herman JP, D'Alessio DA, Woods SC, Seeley RJ (2011) Hyperphagia and increased fat accumulation in two models of chronic CNS glucagon-like peptide-1 loss of function. J Neurosci 31:3904-3913.

Breisch ST, Zemlan FP, Hoebel BG (1976) Hyperphagia and obesity following serotonin depletion by intraventricular p-chlorophenylalanine. Science 192:382-385.

Cabou C, Campistron G, Marsollier N, Leloup C, Cruciani-Guglielmacci C, Penicaud L, Drucker DJ, Magnan C, Burcelin R (2008) Brain glucagon-like peptide-1 regulates arterial blood flow, heart rate, and insulin sensitivity. Diabetes 57:2577-2587.

Cano G, Card JP, Rinaman L, Sved AF (2000) Connections of Barrington's nucleus to the sympathetic nervous system in rats. J Auton Nerv Syst 79:117-128.

Cano G, Mochizuki T, Saper CB (2008) Neural circuitry of stress-induced insomnia in rats. J Neurosci 28:10167-10184.

Cano G, Passerin AM, Schiltz JC, Card JP, Morrison SF, Sved AF (2003) Anatomical substrates for the central control of sympathetic outflow to interscapular adipose tissue during cold exposure. J Comp Neurol 460:303-326.

During MJ, Cao L, Zuzga DS, Francis JS, Fitzsimons HL, Jiao X, Bland RJ, Klugmann M, Banks WA, Drucker DJ, Haile CN (2003) Glucagon-like peptide-1 receptor is involved in learning and neuroprotection. Nat Med 9:1173-1179.

Fenwick NM, Martin CL, Llewellyn-Smith IJ (2006) Immunoreactivity for cocaine- and amphetamine-regulated transcript in rat sympathetic preganglionic neurons projecting to sympathetic ganglia and the adrenal medulla. J Comp Neurol 495:422-433.

Gnanamanickam GJ, Llewellyn-Smith IJ (2011) Innervation of the rat uterus at estrus: a study in full-thickness, immunoperoxidase-stained whole-mount preparations. The Journal of comparative neurology 519:621-643.

Goke R, Larsen PJ, Mikkelsen JD, Sheikh SP (1995) Distribution of GLP-1 binding sites in the rat brain: evidence that exendin-4 is a ligand of brain GLP-1 binding sites. Eur J Neurosci 7:2294-2300.

Grill HJ, Carmody JS, Amanda Sadacca L, Williams DL, Kaplan JM (2004) Attenuation of lipopolysaccharide anorexia by antagonism of caudal brain stem but not forebrain GLP-1-R. Am J Physiol Regul Integr Comp Physiol 287:R1190-1193.

Guo JJ, Browning KN, Rogers RC, Travagli RA (2001) Catecholaminergic neurons in rat dorsal motor nucleus of vagus project selectively to gastric corpus. Am J Physiol Gastrointest Liver Physiol 280:G361-367.

Guyenet PG (2006) The sympathetic control of blood pressure. Nat Rev Neurosci 7:335-346.

Halford JC, Boyland EJ, Blundell JE, Kirkham TC, Harrold JA (2010) Pharmacological management of appetite expression in obesity. Nat Rev Endocrinol 6:255-269.

Hayes MR, Bradley L, Grill HJ (2009) Endogenous hindbrain glucagon-like peptide-1 receptor activation contributes to the control of food intake by mediating gastric satiation signaling. Endocrinology 150:2654-2659.

Hayes MR, Skibicka KP, Grill HJ (2008) Caudal brainstem processing is sufficient for behavioral, sympathetic, and parasympathetic responses driven by peripheral and

hindbrain glucagon-like-peptide-1 receptor stimulation. Endocrinology 149:4059-4068.

Hisadome K, Reimann F, Gribble FM, Trapp S (2010) Leptin directly depolarizes preproglucagon neurons in the nucleus tractus solitarius: electrical properties of glucagon-like Peptide 1 neurons. Diabetes 59:1890-1898.

Hisadome K, Reimann F, Gribble FM, Trapp S (2011) CCK Stimulation of GLP-1 Neurons Involves {alpha}1-Adrenoceptor-Mediated Increase in Glutamatergic Synaptic Inputs. Diabetes 60:2701-2709.

Holmes GM, Browning KN, Tong M, Qualls-Creekmore E, Travagli RA (2009) Vagally mediated effects of glucagon-like peptide 1: in vitro and in vivo gastric actions. J Physiol 587:4749-4759.

Holst JJ (2007) The physiology of glucagon-like peptide 1. Physiol Rev 87:1409-1439.

Jin SL, Han VK, Simmons JG, Towle AC, Lauder JM, Lund PK (1988) Distribution of glucagonlike peptide I (GLP-I), glucagon, and glicentin in the rat brain: an immunocytochemical study. J Comp Neurol 271:519-532.

Kinzig KP, D'Alessio DA, Seeley RJ (2002) The diverse roles of specific GLP-1 receptors in the control of food intake and the response to visceral illness. J Neurosci 22:10470-10476.

Kopf BS, Langhans W, Geary N, Asarian L (2010) Serotonin 2C receptor signaling in a diffuse neuronal network is necessary for LPS anorexia. Brain Res 1306:77-84.

Lam DD, Garfield AS, Marston OJ, Shaw J, Heisler LK (2010) Brain serotonin system in the coordination of food intake and body weight. Pharmacol Biochem Behav 97:84-91.

Langhans W (2007) Signals generating anorexia during acute illness. Proc Nutr Soc 66:321-330.

Larsen PJ, Tang-Christensen M, Holst JJ, Orskov C (1997) Distribution of glucagon-like peptide-1 and other preproglucagon-derived peptides in the rat hypothalamus and brainstem. Neuroscience 77:257-270.

Llewellyn-Smith IJ, Dicarlo SE, Collins HL, Keast JR (2005) Enkephalin-immunoreactive interneurons extensively innervate sympathetic preganglionic neurons regulating the pelvic viscera. J Comp Neurol 488:278-289.

Llewellyn-Smith IJ, Kellett DO, Jordan D, Browning KN, Travagli RA (2012) Oxytocin-immunoreactive innervation of identified neurons in the rat dorsal vagal complex. Neurogastroenterol Motil 24:e136-146.

Llewellyn-Smith IJ, Martin CL, Arnolda LF, Minson JB (1999) Retrogradely transported CTB-saporin kills sympathetic preganglionic neurons. Neuroreport 10:307-312.

Llewellyn-Smith IJ, Reimann F, Gribble FM, Trapp S (2011) Preproglucagon neurons project widely to autonomic control areas in the mouse brain. Neuroscience 180:111-121.

Marina N, Abdala AP, Korsak A, Simms AE, Allen AM, Paton JF, Gourine AV (2011) Control of sympathetic vasomotor tone by catecholaminergic C1 neurones of the rostral ventrolateral medulla oblongata. Cardiovasc Res 91:703-710.

Merchenthaler I, Lane M, Shughrue P (1999) Distribution of pre-pro-glucagon and glucagon-like peptide-1 receptor messenger RNAs in the rat central nervous system. J Comp Neurol 403:261-280.

Morrison SF, Nakamura K, Madden CJ (2008) Central control of thermogenesis in mammals. Exp Physiol 93:773-797.

Nangle MR, Proietto J, Keast JR (2009) Impaired cavernous reinnervation after penile nerve injury in rats with features of the metabolic syndrome. The journal of sexual medicine 6:3032-3044.

Pilowsky P, Llewellyn-Smith IJ, Lipski J, Chalmers J (1992) Substance P immunoreactive boutons form synapses with feline sympathetic preganglionic neurons. J Comp Neurol 320:121-135.

Ray RS, Corcoran AE, Brust RD, Kim JC, Richerson GB, Nattie E, Dymecki SM (2011) Impaired respiratory and body temperature control upon acute serotonergic neuron inhibition. Science 333:637-642.

Reimann F, Habib AM, Tolhurst G, Parker HE, Rogers GJ, Gribble FM (2008) Glucose sensing in L cells: a primary cell study. Cell Metab 8:532-539.

Rinaman L (1999) Interoceptive stress activates glucagon-like peptide-1 neurons that project to the hypothalamus. Am J Physiol 277:R582-590.

Rinaman L (2001) Postnatal development of catecholamine inputs to the paraventricular nucleus of the hypothalamus in rats. The Journal of comparative neurology 438:411-422.

Sandoval DA, Bagnol D, Woods SC, D'Alessio DA, Seeley RJ (2008) Arcuate glucagon-like peptide 1 receptors regulate glucose homeostasis but not food intake. Diabetes 57:2046-2054.

Sara SJ (2009) The locus coeruleus and noradrenergic modulation of cognition. Nat Rev Neurosci 10:211-223.

Sasaki M (2005) Role of Barrington's nucleus in micturition. J Comp Neurol 493:21-26.

Sawchenko PE, Swanson LW (1982) The organization of noradrenergic pathways from the brainstem to the paraventricular and supraoptic nuclei in the rat. Brain research 257:275-325.

Schreihofer AM, Sved AF (2011) The ventrolateral medulla and sympathetic regulation of arterial pressure. In: Central regulation of autonomic functions(Llewellyn-Smith, I. J. and Verberne, A. J. M., eds), pp 78-97 New York: Oxford University Press.

Shughrue PJ, Lane MV, Merchenthaler I (1996) Glucagon-like peptide-1 receptor (GLP1-R) mRNA in the rat hypothalamus. Endocrinology 137:5159-5162.

Skibicka KP, Alhadeff AL, Grill HJ (2009) Hindbrain cocaine- and amphetamine-regulated transcript induces hypothermia mediated by GLP-1 receptors. J Neurosci 29:6973-6981.

Tang-Christensen M, Larsen PJ, Goke R, Fink-Jensen A, Jessop DS, Moller M, Sheikh SP (1996) Central administration of GLP-1-(7-36) amide inhibits food and water intake in rats. Am J Physiol 271:R848-856.

Tauchi M, Zhang R, D'Alessio DA, Stern JE, Herman JP (2008) Distribution of glucagon-like peptide-1 immunoreactivity in the hypothalamic paraventricular and supraoptic nuclei. J Chem Neuroanat 36:144-149.

Thiele TE, Seeley RJ, D'Alessio D, Eng J, Bernstein IL, Woods SC, van Dijk G (1998) Central infusion of glucagon-like peptide-1-(7-36) amide (GLP-1) receptor antagonist attenuates lithium chloride-induced c-Fos induction in rat brainstem. Brain Res 801:164-170.

Thorens B, Widmann C (1996) Signal transduction and desensitization of the glucagon-like peptide-1 receptor. Acta Physiol Scand 157:317-319.

Trapp S, Hisadome K (2011) Glucagon-like peptide 1 and the brain: central actions-central sources? Auton Neurosci 161:14-19.

Travagli RA, Hermann GE, Browning KN, Rogers RC (2006) Brainstem circuits regulating gastric function. Annu Rev Physiol 68:279-305.

Turton MD, O'Shea D, Gunn I, Beak SA, Edwards CM, Meeran K, Choi SJ, Taylor GM, Heath MM, Lambert PD, Wilding JP, Smith DM, Ghatei MA, Herbert J, Bloom SR (1996) A role for glucagon-like peptide-1 in the central regulation of feeding. Nature 379:69-72.

Van Dijk G, Thiele TE, Donahey JC, Campfield LA, Smith FJ, Burn P, Bernstein IL, Woods SC, Seeley RJ (1996) Central infusions of leptin and GLP-1-(7-36) amide differentially stimulate c-FLI in the rat brain. Am J Physiol 271:R1096-1100.

Vrang N, Hansen M, Larsen PJ, Tang-Christensen M (2007) Characterization of brainstem preproglucagon projections to the paraventricular and dorsomedial hypothalamic nuclei. Brain Res 1149:118-126.

Wan S, Browning KN, Travagli RA (2007a) Glucagon-like peptide-1 modulates synaptic transmission to identified pancreas-projecting vagal motoneurons. Peptides 28:2184-2191.

Wan S, Coleman FH, Travagli RA (2007b) Glucagon-like peptide-1 excites pancreas-projecting preganglionic vagal motoneurons. Am J Physiol Gastrointest Liver Physiol 292:G1474-1482.

Williams DL, Baskin DG, Schwartz MW (2009) Evidence that intestinal glucagon-like peptide-1 plays a physiological role in satiety. Endocrinology 150:1680-1687.

Yamamoto H, Kishi T, Lee CE, Choi BJ, Fang H, Hollenberg AN, Drucker DJ, Elmquist JK (2003) Glucagon-like peptide-1-responsive catecholamine neurons in the area postrema link peripheral glucagon-like peptide-1 with central autonomic control sites. J Neurosci 23:2939-2946.

Yamamoto H, Lee CE, Marcus JN, Williams TD, Overton JM, Lopez ME, Hollenberg AN, Baggio L, Saper CB, Drucker DJ, Elmquist JK (2002) Glucagon-like peptide-1 receptor stimulation increases blood pressure and heart rate and activates autonomic regulatory neurons. J Clin Invest 110:43-52.

Figure 1 online & print
Click here to download high resolution image

AP: 1/6 (17%)

AP

NTS

NTS: 7/16 (44%)

HGN

DMV: 11/16 (69%)

AP: 4/102 (4%)

AP

NTS

NTS: 20/50 (40%)

HGN

DMV: 26/70 (37%)

AP

NTS

AP: 1/5 (20%)

NTS: 20/32 (63%)

HGN

DMV: 11/35 (31%)

AP: 5/41 (12%)

AP

NTS

NTS: 10/42 (24%)

HGN

DMV: 23/66 (35%)

AP: 3/50 (6%)

AP

NTS

NTS: 11/43 (26%)

HGN

DMV: 22/71 (31%)

AP: 1/14 (7%)

AP

NTS

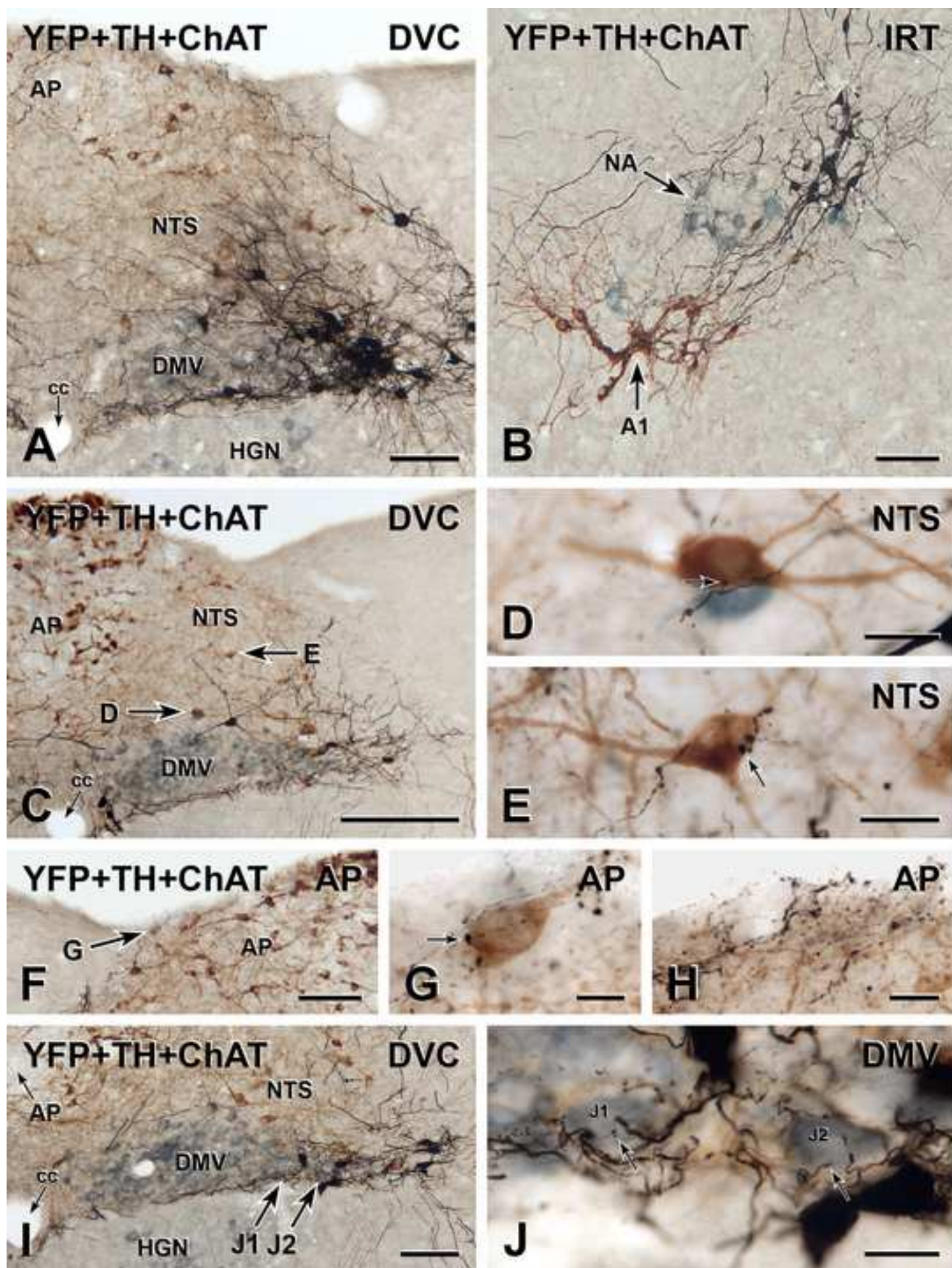NTS: 12/32 (38%)
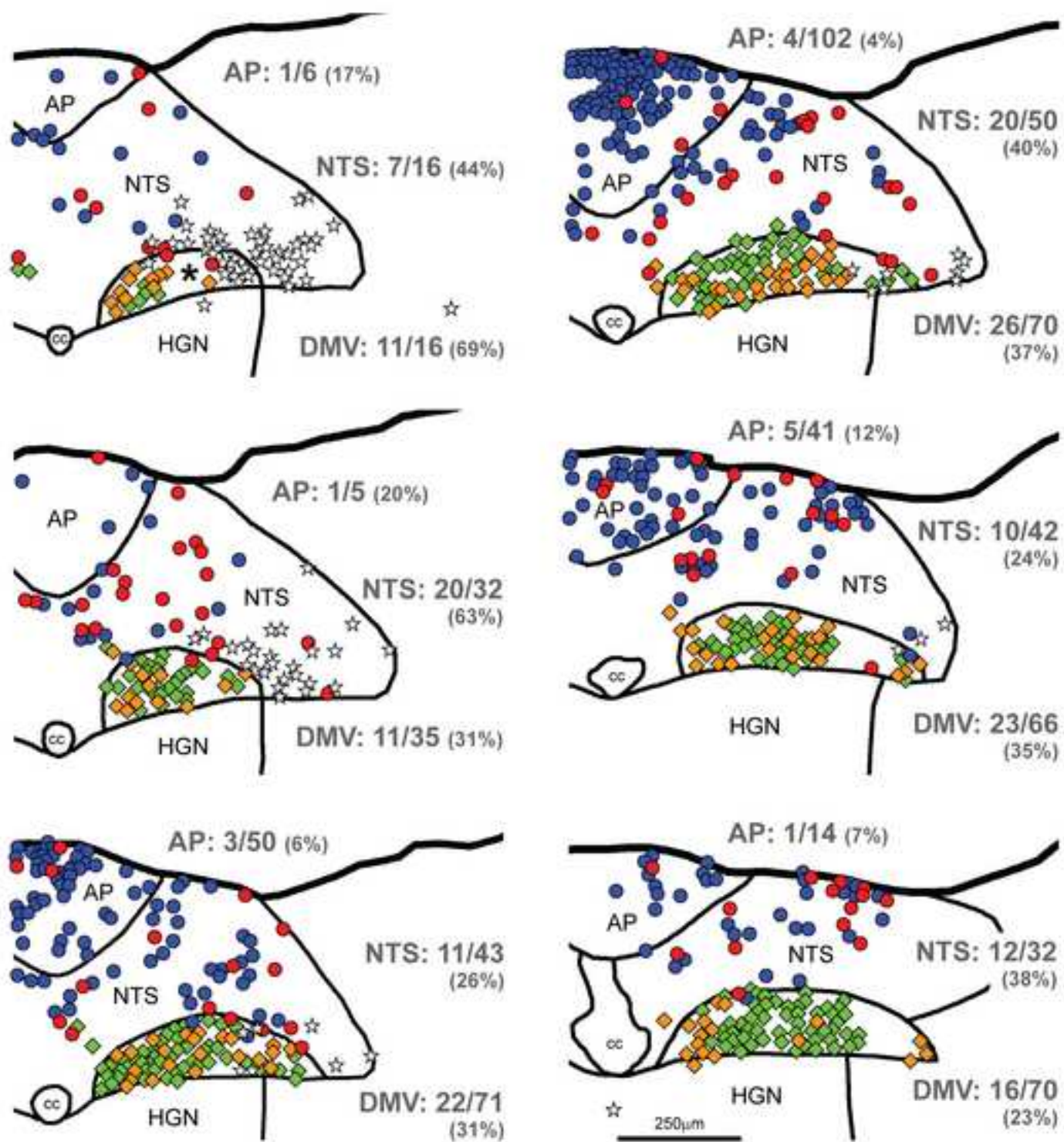
HGN

DMV: 16/70 (23%)

250µm

Figure 3 online
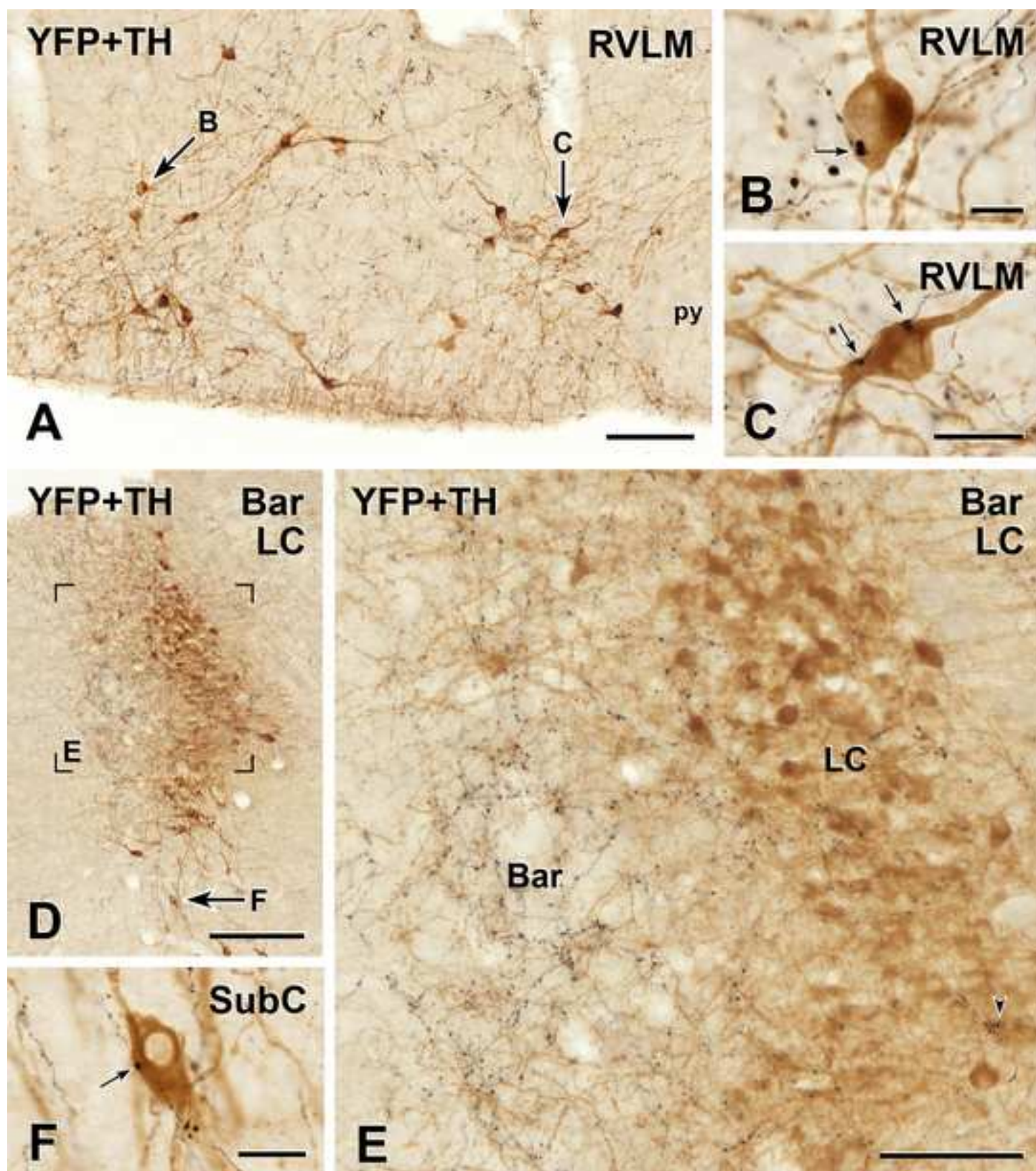**Click here to download high resolution image**

Figure 4 online
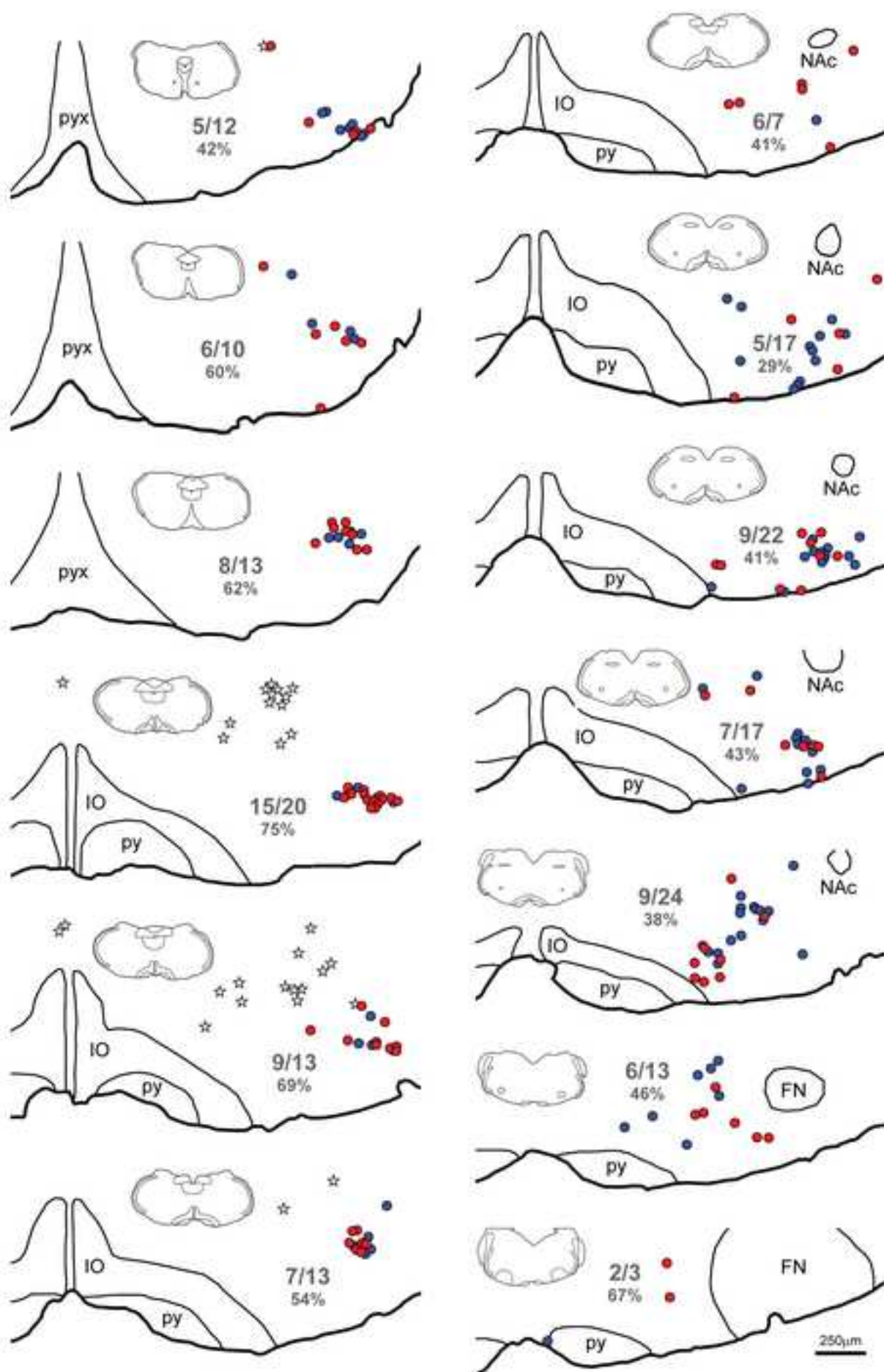**Click here to download high resolution image**

Figure 5 online
Click here to download high resolution image

Figure 6 online
Click here to download high resolution image

Total: 9/16 (56%)

Total: 29/49 (59%)
NAc
RPa: 23/38 (61%)
PPY: 5/9 (56%)

Total: 6/7 (86%)

NAc
Total: 29/51 (57%)
RPa: 10/20 (50%)
PPY: 19/27 (70%)

Total: 29/39 (74%)
RPa: 15/20 (75%)
VS: 13/15 (87%)

Total: 25/46 (54%)
Midline: 13/26 (50%)
Lateral: 12/19 (63%)
FN

Total: 35/54 (65%)
NAc
RPa: 18/34 (53%)
PPY: 13/14 (93%)

Total: 10/24 (42%)   FN

250μm

AP: 1/6 (17%)

AP

NTS

NTS: 7/16 (44%)

HGN

CC

DMV: 11/16 (69%)

AP: 4/102 (4%)

AP

NTS

NTS: 20/50 (40%)

CC

HGN

DMV: 26/70 (37%)

AP

NTS

AP: 1/5 (20%)

NTS: 20/32 (63%)

CC

HGN

DMV: 11/35 (31%)

AP: 5/41 (12%)

AP

NTS

NTS: 10/42 (24%)

CC

HGN

DMV: 23/66 (35%)

AP: 3/50 (6%)

AP

NTS

NTS: 11/43 (26%)

CC

HGN

DMV: 22/71 (31%)

AP: 1/14 (7%)

AP

NTS

NTS: 12/32 (38%)

CC

HGN

250µm

DMV: 16/70 (23%)

Figure 3 print
Click here to download high resolution image

Figure 4 print
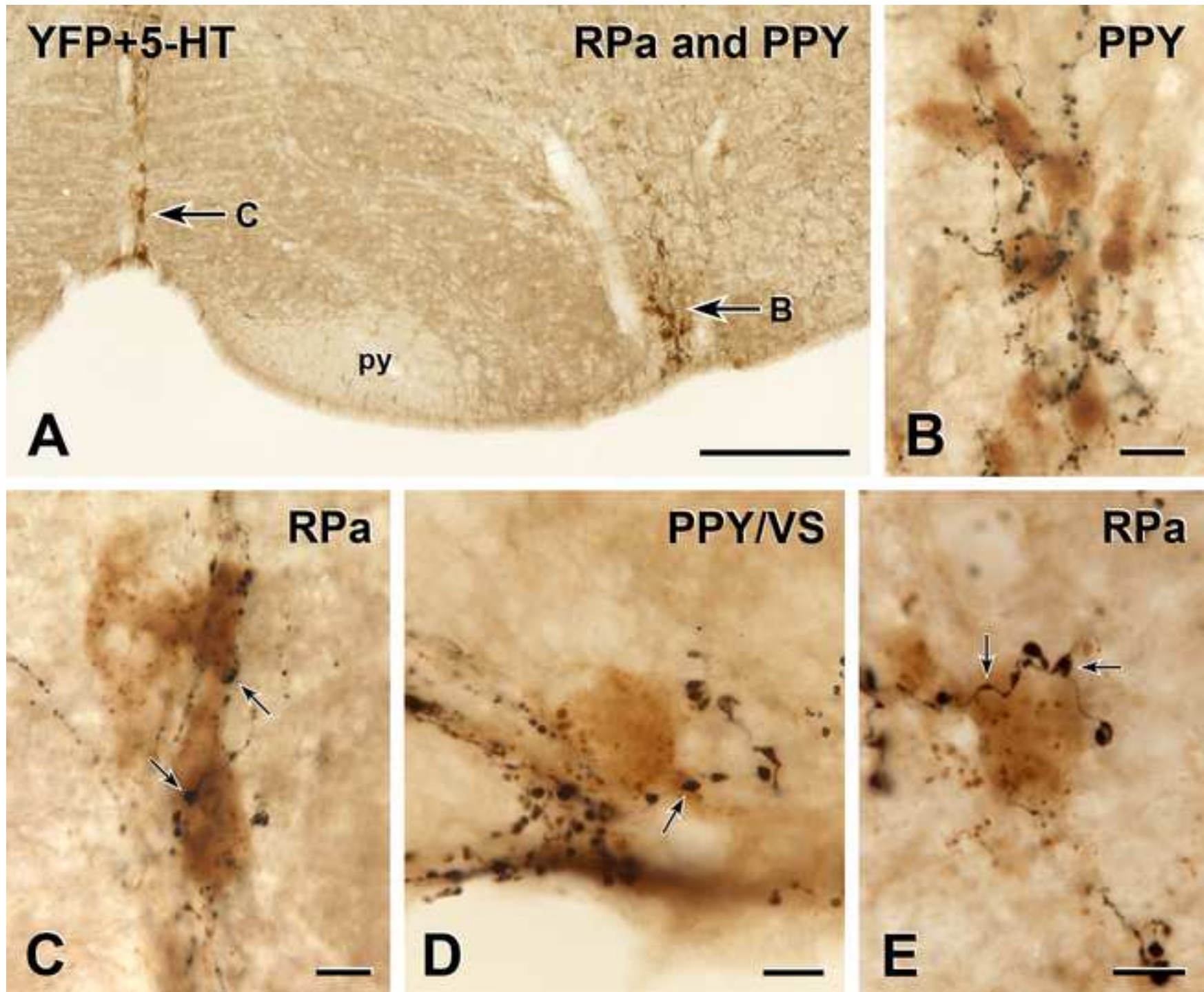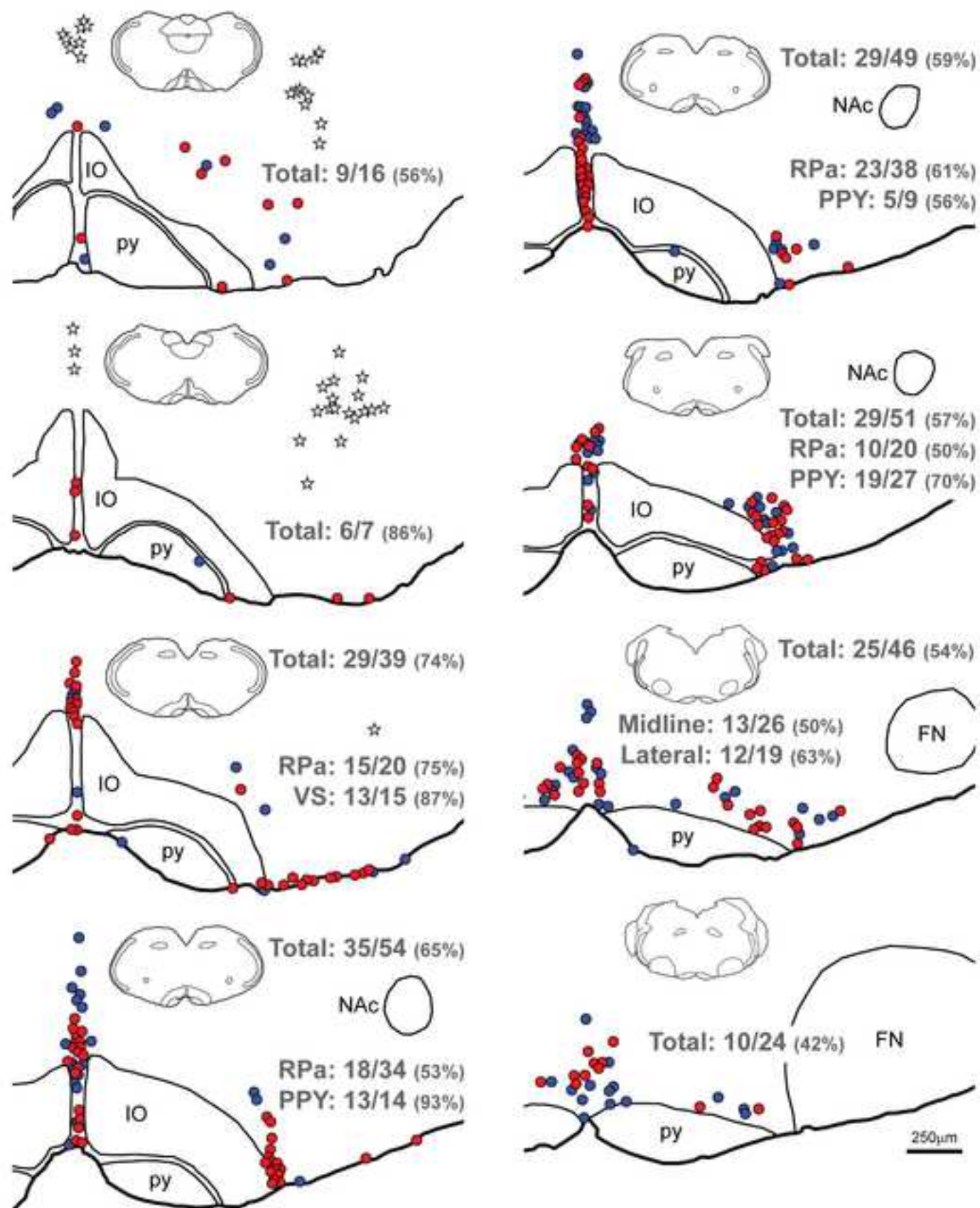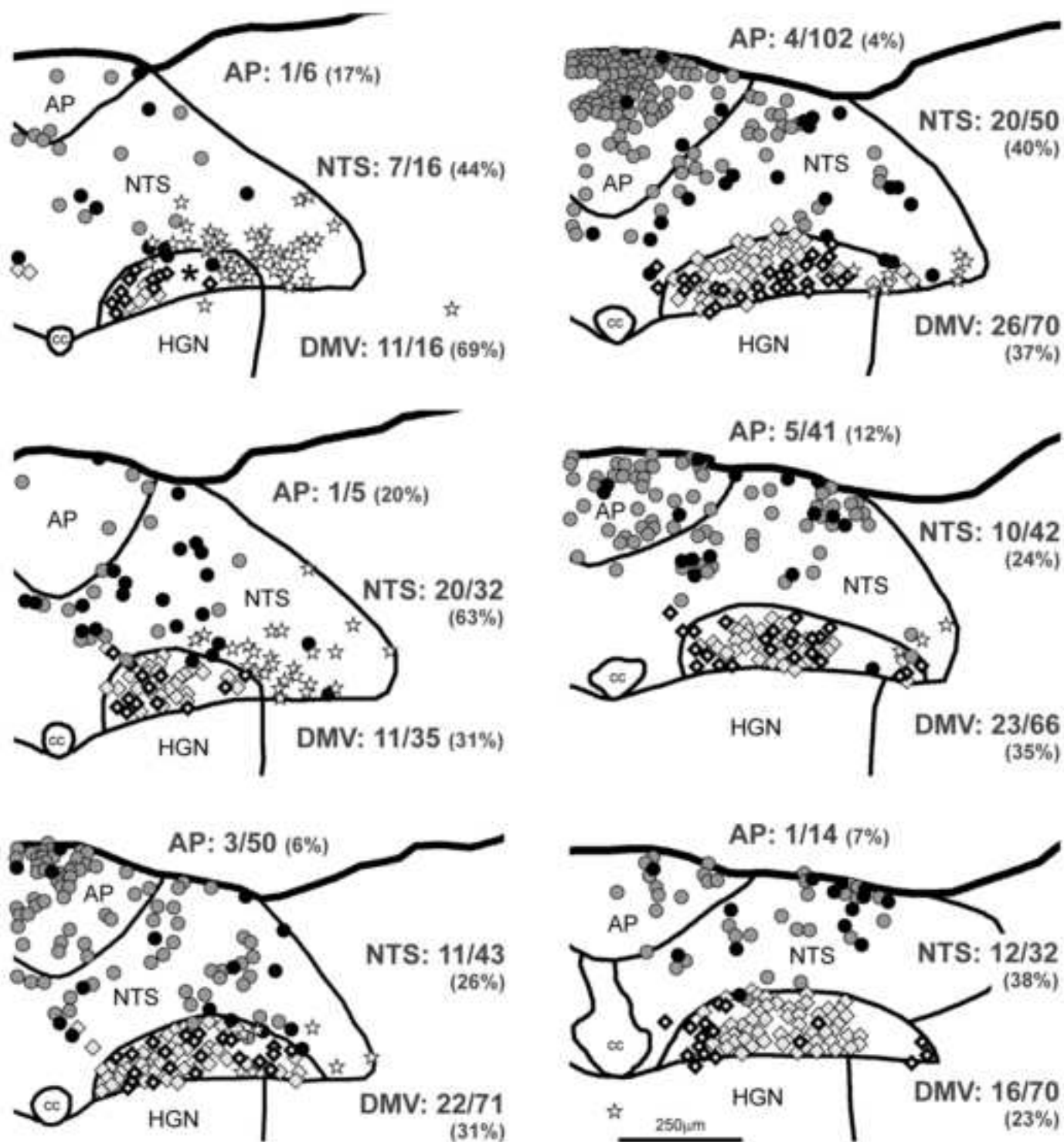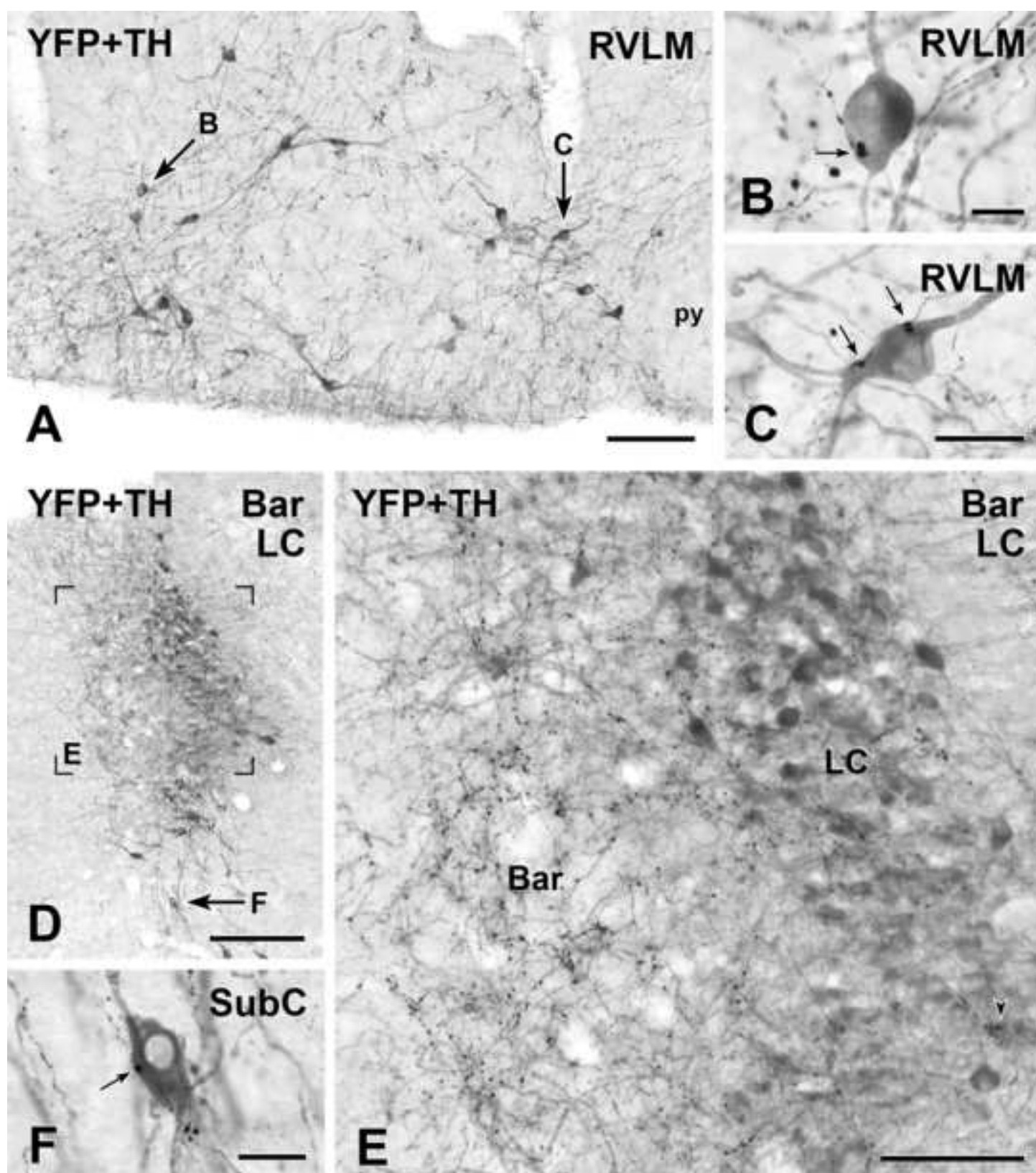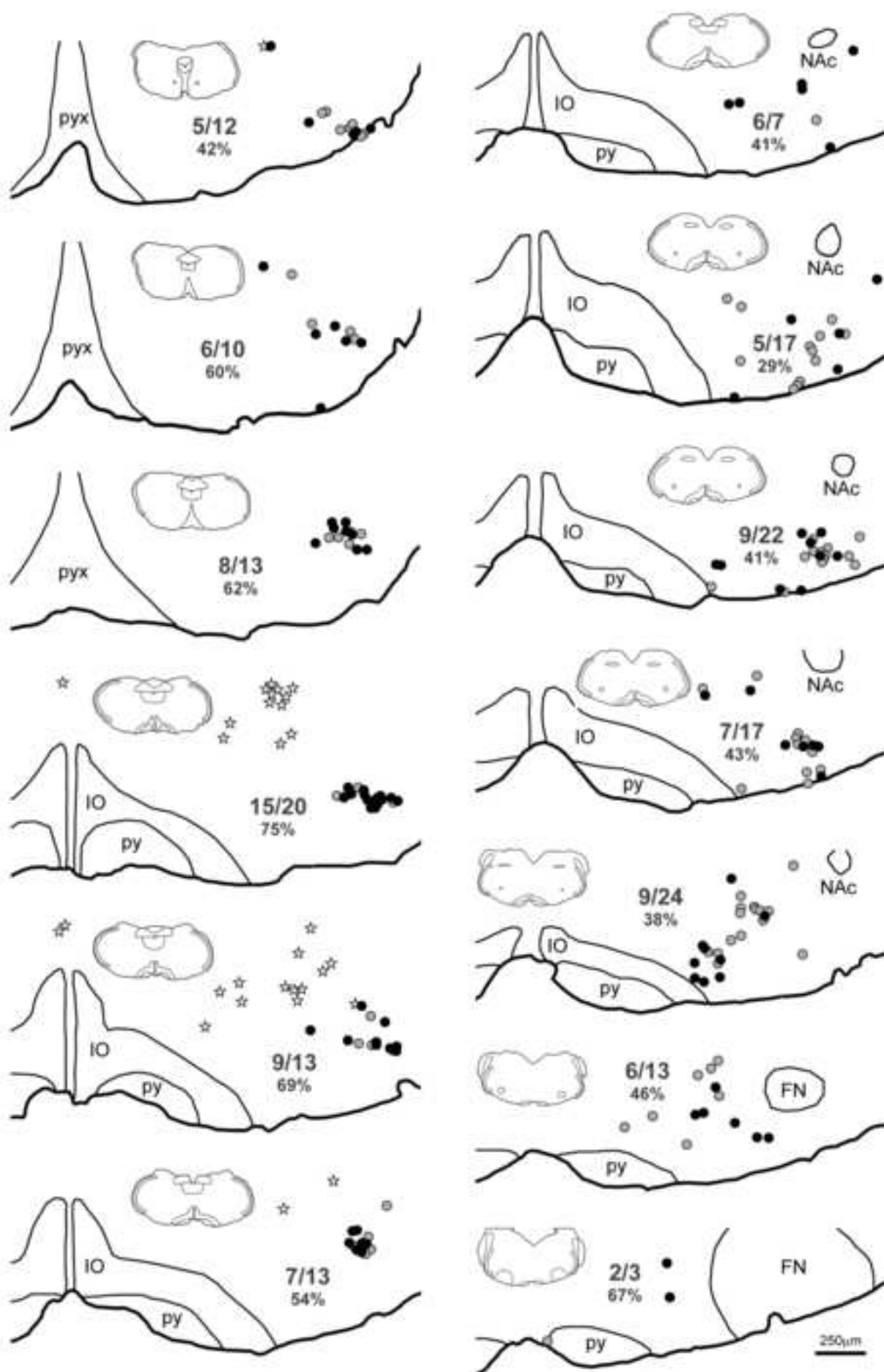**Click here to download high resolution image**

Figure 5 print
Click here to download high resolution image

Figure 6 print
Click here to download high resolution image

Total: 9/16 (56%)

IO

py

Total: 29/49 (59%)

NAc

RPa: 23/38 (61%)
PPY: 5/9 (56%)

IO

py

Total: 6/7 (86%)

IO

py

NAc

Total: 29/51 (57%)
RPa: 10/20 (50%)
PPY: 19/27 (70%)

IO

py

Total: 29/39 (74%)

RPa: 15/20 (75%)
VS: 13/15 (87%)

IO

py

Total: 25/46 (54%)

Midline: 13/26 (50%)
Lateral: 12/19 (63%)

FN

py

Total: 35/54 (65%)

NAc

RPa: 18/34 (53%)
PPY: 13/14 (93%)

IO

py

Total: 10/24 (42%)   FN

py

250μm